

1 **Reconstructed soil moisture droughts in Belgium reveal** 2 **2011–2020 was the driest decade since 1970**

3 Katoria Lekarkar*¹, Oldrich Rakovec², Rohini Kumar³, Stefaan Dondeyne^{1,4,6}, and Ann van
4 Griensven^{1,5}

5 ¹Department of Water and Climate, Vrije Universiteit Brussel, Pleinlaan 2, 1050 Brussels, Belgium

6 ²UFZ-Helmholtz Centre for Environmental Research, Permoserstraße 15, 04318 Leipzig, Germany

7 ³Faculty of Environmental Sciences, Czech University of Life Sciences Prague, Praha-Suchbát, Czech Republic

8 ⁴Gembloux Agro-Bio Tech, University of Liège, Pass. des Déportés 2, 5030 Gembloux, Belgium

9 ⁵Water Science & Engineering Department, IHE Delft Institute for Water Education, 2611 AX Delft, The Netherlands

10 ⁶Department of Soil Science and Land Resources, Universitas Padjadjaran, Jawa Barat 45363, Bandung, Indonesia

11 **Abstract**

12 In recent years, Belgium has experienced a sequence of intense droughts with wide-ranging
13 impacts across multiple sectors. Determining whether these events are unprecedented or within
14 natural variability requires indicators that properly diagnose drought. Root-zone soil moisture is
15 a suitable indicator because it integrates meteorological forcings with land-surface processes. In
16 Belgium, however, operational monitoring relies mainly on precipitation-based indices and lacks
17 long-term in situ soil-moisture observations, leaving uncertainty about whether these indices capture
18 the persistence of root-zone drought. To address this gap, we reconstructed daily root-zone soil-
19 moisture dynamics over Belgium for 1970–2020 using the mesoscale Hydrologic Model (mHM),
20 placing recent droughts in historical context and evaluating the adequacy of precipitation-based
21 indicators for representing drought conditions. Our analysis shows that droughts in 2011–2020
22 were unprecedented in both duration and severity over the past five decades. Between 2011 and
23 2020, the country experienced a cumulative three years (non-consecutive) of drought exposure,
24 representing 30% of the decade. This more than doubles the cumulative duration in each decade
25 from 1981–2010 and about 1.5 times that of 1971–1980.

26 We further find that the Standardized Precipitation–Evapotranspiration Index (SPEI), currently
27 used operationally as a proxy for agricultural droughts in Belgium, underestimates the persistence
28 of root-zone droughts because it does not explicitly account for land-surface memory. Thus, by
29 including soil moisture monitoring in drought assessment, residual stresses on agriculture and
30 subsurface water, which can persist long after meteorological conditions have normalized, can still
31 be detected. This gives decision-makers a more realistic understanding of droughts and how to
32 respond proportionately.

33 **Keywords**— Mesoscale, climate variability, drought persistence, cumulative exposure, agricul-
34 tural drought monitoring

*Corresponding author: katoria.lesaalon.lekarkar@vub.be

1 Introduction

Belgium has experienced a succession of severe droughts in recent years, with major impacts on agriculture, water resources, and inland navigation, resulting in economic losses amounting to hundreds of millions of euros (De Ridder et al., 2020; Tröltzsch et al., 2016).

The cross-sectoral impacts of the successive droughts of 2016–2017 and 2018–2019 were particularly significant. To demonstrate, in the Flemish Region¹, the 2018–2019 drought caused widespread crop losses, prompting farmers to submit compensation claims of about €150 million to the Flemish Disaster Fund (De Ridder et al., 2020). Low water levels arising from the drought also disrupted inland navigation and caused an estimated €283 million in economic damage (De Vlaamse Waterweg nv, 2022). In the Walloon Region, the drought similarly affected agriculture and water availability, and the period from June to August 2018 was officially recognized as an agricultural disaster, with about €31.5 million allocated in compensation to affected farmers (Le sillon Belge, 2019; Thibaut et al., 2023). Similar impacts were experienced during another drought in 2022, where at the peak of the drought in July that year, the country received only 5 mm of precipitation, the lowest monthly total for July in 137 years (since 1885). Groundwater levels in Belgium consequently fell to their lowest levels since at least 2000 (DOV, 2025; Piézométrie du Service Public de Wallonie, 2025), and in many locations they did not fully recover during the following winter (VMM, 2023).

Although the impacts of these recent droughts are well documented, their significance in a longer climatological context remains unclear. In particular, it is not yet known whether the recent clustering of severe droughts represents a departure from earlier decades or falls within the range of natural climate variability in Belgium. Addressing this question requires a reconstruction of drought occurrence over a sufficiently long period, based on indicators that adequately capture the propagation and persistence of drought within the hydrological system.

Drought is characterized in several ways; in this manuscript we focus on three commonly used forms. Meteorological drought describes a persistence of precipitation shortage, agricultural drought refers to a sustained deficit in soil moisture which causes plant water stress, while hydrological drought indicates shortages in surface and subsurface water supplies (Mishra & Singh, 2010). In Belgium there is an extensive network of precipitation, river discharge and groundwater monitoring stations which provide the basis for monitoring hydrological and meteorological droughts. This data underlies the drought indices found in dedicated platforms for tracking and communicating the evolution of droughts across the country (e.g. <https://www.meteo.be/en/weather/forecasts/drought>, <https://vmm.vlaanderen.be/water/droogte>). Due to the lack of long-term observations of soil moisture in the country, the extent of agricultural droughts is presently evaluated with the Standardized Precipitation Evaporation Index (SPEI) (Vicente-Serrano et al., 2010) which expresses anomalies in the climatic water balance, that is, precipitation minus potential evapotranspiration. The nationwide drought conditions are reported through <https://www.meteo.be/en/weather/forecasts/drought>.

Although useful, precipitation- and temperature-based drought indices are constrained by their limited ability to fully represent agricultural drought conditions. Firstly, these indices do not explicitly account for the vertical distribution of water within the root zone that supports plant

¹Belgium is divided into three administrative regions: the Flemish Region (Flanders), the Brussels-Capital Region, and the Walloon Region https://www.belgium.be/en/about_belgium/government/regions.

75 growth, nor do they reflect the complex interactions between soil moisture and vegetation across
76 different stages of plant development and are thus inadequate to represent extreme water shortage
77 that would lead to biomass and crop yield reduction (Mishra & Singh, 2010; Samaniego et al., 2013;
78 Sheffield et al., 2004). While soil moisture may exhibit a direct link to precipitation at monthly
79 timescales, soil moisture responses can be nonlinear at shorter timescales, particularly during dry
80 conditions. Soil moisture also has a memory effect that can lag precipitation anomalies by days
81 to months and in turn prolong the persistence and severity of drought (Bonan & Stillwell-Soller,
82 1998; Nicholson, 2000; Seneviratne et al., 2006; Wu et al., 2002). Accordingly, developing indices
83 based on soil moisture offers a more reliable indicator of agricultural drought, as soil moisture
84 integrates the effects of antecedent precipitation, plant water uptake through transpiration, and the
85 increasing persistence of soil wetness with soil depth (Sheffield et al., 2004; Wu et al., 2002).

86 The goal of this study is therefore to produce a retrospective high-resolution reconstruction
87 of root-zone soil moisture and use it to provide a first assessment of soil-moisture droughts in
88 Belgium over the five decades from 1970 to 2020. We aim to characterize major droughts that
89 have occurred over this period by clustering soil moisture anomalies using thresholds that capture
90 the spatiotemporal characteristics of identified events and rank them based on their magnitude,
91 spatial extent and duration, and evaluate how drought patterns in the country have evolved over the
92 five decades. To evaluate the correspondence between SPEI and soil moisture-based anomalies
93 to represent agricultural droughts, we compare SPEI at different accumulation periods to a soil
94 moisture index (SMI) (Samaniego et al., 2018) during selected major drought events.

95 **2 Methodology**

96 **2.1 Study domain**

97 Belgium is located in Western Europe covering an area of 30,528 km², varying in topography from
98 sea level along the North Sea coast to 700 m in the Ardennes-Eifel massif in the south eastern
99 parts (Figure 1) (Meersmans et al., 2016; Sousa-Silva et al., 2016). The country experiences
100 a warm temperate maritime climate (Köppen-Geiger Cfb) strongly modulated by the warming
101 effect of the North Atlantic Drift (Beck et al., 2023; Erpicum et al., 2018). Data from the Royal
102 Meteorological Institute of Belgium (RMI) shows that mean annual temperature ranges between
103 13 and 17 °C, varying spatially with elevation and distance inland. Winters are generally mild, with
104 December–January lows dipping under 5 °C but rarely below freezing conditions for long periods.
105 Winters are colder in the Ardennes region due to a weaker maritime influence and higher elevation.
106 Summers are moderately warm with July highs peaking around 18 °C although extremes above
107 30 °C have occurred in recent years. The country receives an annual average precipitation of about
108 800 mm which varies between 700 mm in the western low lying regions, up to 1400 mm in the
109 Ardennes where precipitation is enhanced by orographic effects (Erpicum et al., 2018). Temporally,
110 rainfall is fairly evenly distributed throughout the year (Figure 1), with seasonal patterns dominated
111 by summer convective storms and winter frontal systems (Brisson et al., 2011; Goudenhoofdt &
112 Delobbe, 2013; Journée et al., 2015).

113 Land cover in the country is predominantly agricultural (44%), dominated by croplands and
114 animal husbandry. Cultivated areas dominate the central loamy belt and the northwest of the

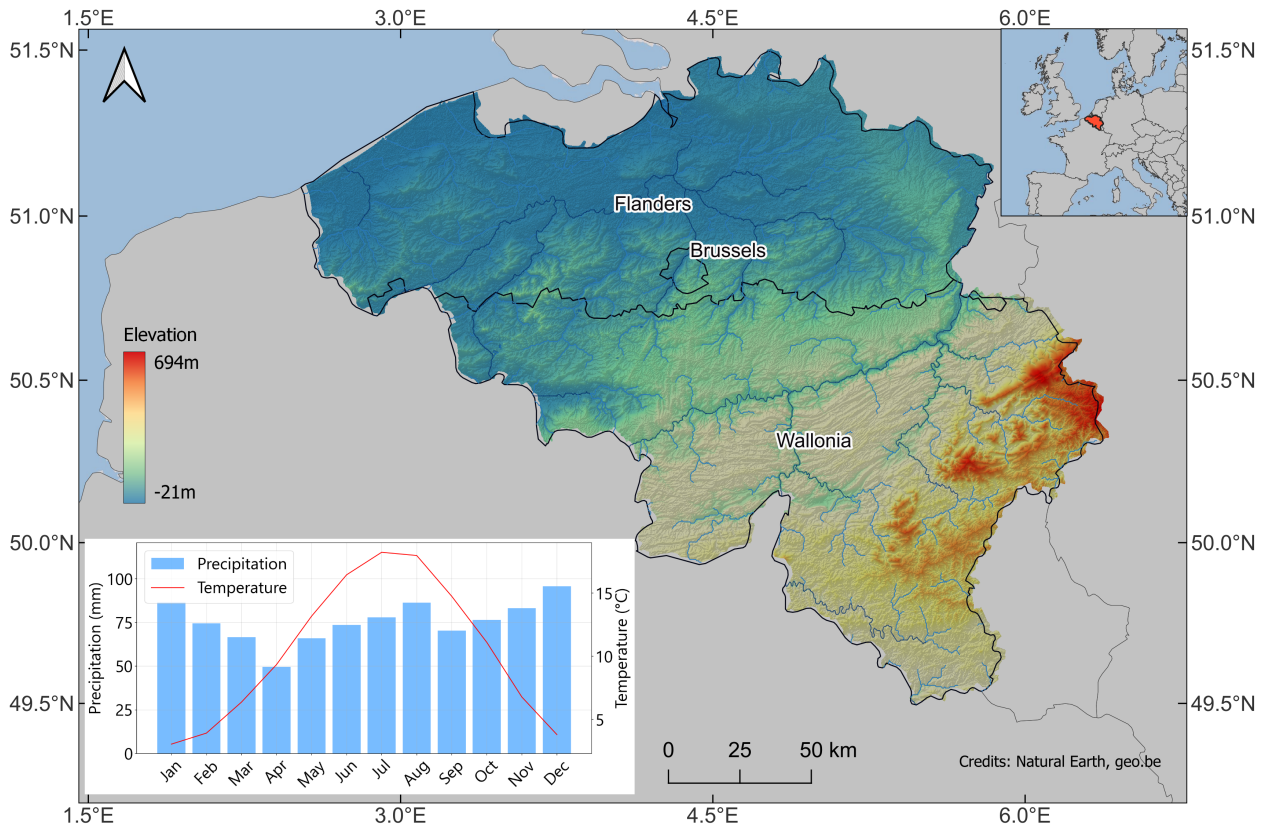


Figure 1: Topographic map of Belgium. The Ardennes region is distinguishable by its high elevation in the south east. Monthly mean precipitation and temperature in the inset plot are derived from data provided by The Royal Meteorological Institute of Belgium for the climatological period 1994-2023.

country while the coastal polders typified by heavy soils, are more suited for animal-based farming (Beckers et al., 2018, 2020; Statbel, 2025a). Forests cover about 23% of the territory (just over 700,000 hectares) with 79.8% in the Walloon region, 19.9% in Flanders and 0.3% in the Brussels-Capital (Royal Forestry Society of Belgium, 2025; Sousa-Silva et al., 2016). Most of the lowland forests are dominated by broad-leaved tree species with clusters of coniferous forest plantations in the north east. In the Ardennes, forests form a mixed broadleaved–coniferous complex in the foothills, gradually transitioning to conifer-dominated stands at higher elevations (Royal Forestry Society of Belgium, 2025; Statbel, 2025a). Built-up and urbanized areas account for about 20% of the land with most cities dating back to the Middle Ages. The average population density of the country is 385 inhabitants/km² (Beckers et al., 2020; Statbel, 2025b).

2.2 The mesoscale Hydrologic Model

In our study, we used the mesoscale Hydrologic Model (mHM; Kumar et al., 2013; Samaniego et al., 2010) (version v-5.13.2-dev0) to simulate domain-wide root-zone (0-2 m) soil moisture conditions and streamflow, which we used as an additional hydrologic constraint for validating basin-scale hydrology at major outlets.

mHM is a spatially distributed hydrological model based on numerical representations of dominant hydrological processes. The model is driven by hourly to daily meteorological forcings,

132 which include precipitation, air temperature (henceforth simply *temperature*), and potential evap-
133 otranspiration, and accounts for major hydrological processes like snowmelt and accumulation,
134 canopy storage, evapotranspiration, surface runoff and flood routing, three-layer soil moisture
135 content, and subsurface storage. To represent spatial variability of inputs and state variables, the
136 model uses three different spatial resolutions, namely (in order of fine to coarse resolution) Level-0
137 (L_0 : small-scale morphology) to represent the main terrain features, geological features, land cover,
138 and soil properties; Level-1 (L_1 : mesoscale hydrology) to represent the dominant hydrological
139 processes; and Level-2 (L_2 : large-scale meteorology) to describe the variability of meteorological
140 forcings. The model harmonizes the data internally using the multiscale parameter regionalization
141 (MPR; Samaniego et al., 2010). MPR links model parameters at L_1 to their corresponding ones at
142 L_0 using non-linear transfer functions that couple catchment characteristics with global (calibration)
143 parameters to regionalize model hydrologic parameters at L_0 and link them to their corresponding
144 values at L_1 using upscaling operators such as arithmetic mean, geometric mean, and harmonic
145 mean (MPR; Livneh et al., 2015). With this technique, mHM achieves quasi scale-invariant param-
146 eters that enable the model to preserve the spatial variability of state variables and conserve mass
147 balance (Kumar et al., 2013; Samaniego et al., 2010, 2011, 2013). mHM has been successfully
148 used in multiple studies at scales ranging from river basins (Banjara et al., 2025; Dembélé et al.,
149 2020; Demirel et al., 2024; Zink et al., 2017), country level (Boeing et al., 2022; Rakovec et al.,
150 2019; Samaniego et al., 2013) up to continental-scale (Kumar et al., 2025; Moravec et al., 2019;
151 Samaniego et al., 2018) and global studies (Řehoř et al., 2025; Shrestha et al., 2025).

152 2.2.1 Input data

153 Our simulation is driven by daily fields of precipitation and temperature from the ENSEMBLES
154 gridded dataset (E-OBS) version 30.0e (Cornes et al., 2018), which covers the entire modelling
155 domain. E-OBS is a daily land-only gridded observational dataset over Europe which blends station
156 network time series from the European National Meteorological and Hydrological Services or other
157 sources and is provided with spatial resolutions of 0.1° and 0.25° . Our setup uses the 0.1° resolution
158 product (access url: [https://cds.climate.copernicus.eu/datasets/insitu-gridded-observations-europe?](https://cds.climate.copernicus.eu/datasets/insitu-gridded-observations-europe?tab=download)
159 [tab=download](https://cds.climate.copernicus.eu/datasets/insitu-gridded-observations-europe?tab=download), last accessed March 2025). Since E-OBS does not provide potential evapotran-
160 spiration data, we generated this from the E-OBS minimum and maximum temperature using the
161 method of Hargreaves and Samani (1985).

162 The morphological datasets for the model originate from different sources, namely, LAI
163 maps from Global Inventory Modeling and Mapping Studies (GIMMS) (Cao et al., 2023), DEM
164 from the Shuttle Radar Topography Mission (Farr et al., 2007), land use data from Corine Land
165 Cover (<https://land.copernicus.eu/en/products/corine-land-cover>), soil texture and bulk density
166 data from the Harmonized World Soil Database (Nachtergaele et al., 2023), and geology datasets
167 from the Global Lithological Map Database (Hartmann & Moosdorf, 2012), accessed from the
168 URL: <https://www.geo.uni-hamburg.de/geologie/forschung/aquatische-geochemie/glim.html> (last
169 accessed February 2025). To ensure the spatial consistency required by mHM, we prepared all
170 L_0 datasets at 0.001953125° ($1/512^\circ$), bilinearly coarsened the L_2 meteorological data to 0.125°
171 ($1/8^\circ$), and set the resolution of L_1 to 0.03125° ($1/32^\circ$), these are summarized in Table 1. We then
172 ran the model from 1965 to 2020, including a warm-up period of 5 years at the beginning.

173 Long-term in situ soil moisture data to validate the soil moisture output of mHM is not available

174 within Belgium, so we expanded the model domain to cover parts of France, Germany and the
 175 Netherlands, where soil moisture observations are available from the International Soil Moisture
 176 Network (ISMN) (Dorigo et al., 2021). From the ISMN, we used data from the following networks:
 177 COSMOS (Zreda et al., 2008), GROW (Xaver et al., 2020), TERENO (Bogena et al., 2018),
 178 BFG_Nw and ORACLE, all shown in Figure 2.

Table 1: Data sources and spatial resolutions used in the mHM setup.

Dataset	Resolution (degrees)	Input format	Source
Meteorological data	1/8	NetCDF	E-OBS v30.0e
Leaf Area Index	1/512	NetCDF	GIMMS
DEM	1/512	ASCII Grid	SRTM
Geology	1/512	ASCII Grid	Global Lithological Map Database
Land Cover	1/512	ASCII Grid	Corine Landcover
Soil texture	1/512	ASCII Grid	Harmonized World Soil Database

179 2.2.2 mHM Soil Moisture simulation

180 mHM calculates water infiltration between soil layers using an exponential function that accounts
 181 for the nonlinearity of soil water retention (Livneh et al., 2015; Samaniego et al., 2010). Briefly,
 182 for a given soil layer, k , on pervious areas, the infiltration I_k into the layer is determined by the
 183 equation:

$$I_k = I_{k-1} * \left(\frac{\theta_k}{\theta_{sat,k}} \right)^{\beta_k} \quad (1)$$

184 I_{k-1} represents the infiltration from the previous layer $k - 1$, θ_k is the soil moisture of layer
 185 k , $\theta_{sat,k}$ is the saturation moisture content for the layer, and β_k is an exponential parameter that
 186 adjusts for the non-linear nature of soil moisture retention. Once infiltration is calculated, the
 187 model updates soil moisture θ_t by adding the difference between the layer infiltration I_t and actual
 188 evapotranspiration (ET_t) for the time step as;

$$\theta_t = \theta_{t-1} + I_t - ET_t \quad (2)$$

189 Actual evapotranspiration is calculated by reducing the potential evapotranspiration (PET)
 190 based on a soil moisture stress factor, f_{SM} , which varies depending on the soil moisture content.

$$ET = f_{roots} \cdot f_{SM} \cdot PET \quad (3)$$

191 f_{roots} is the fraction of roots in the soil horizon and f_{SM} is calculated using either the Feddes
 192 equation (Feddes, 1982):

$$f_{SM} = \frac{\theta - \theta_{pwp}}{\theta_{fc} - \theta_{pwp}} \quad (4)$$

193 or the Jarvis equation (after Jarvis, 1989):

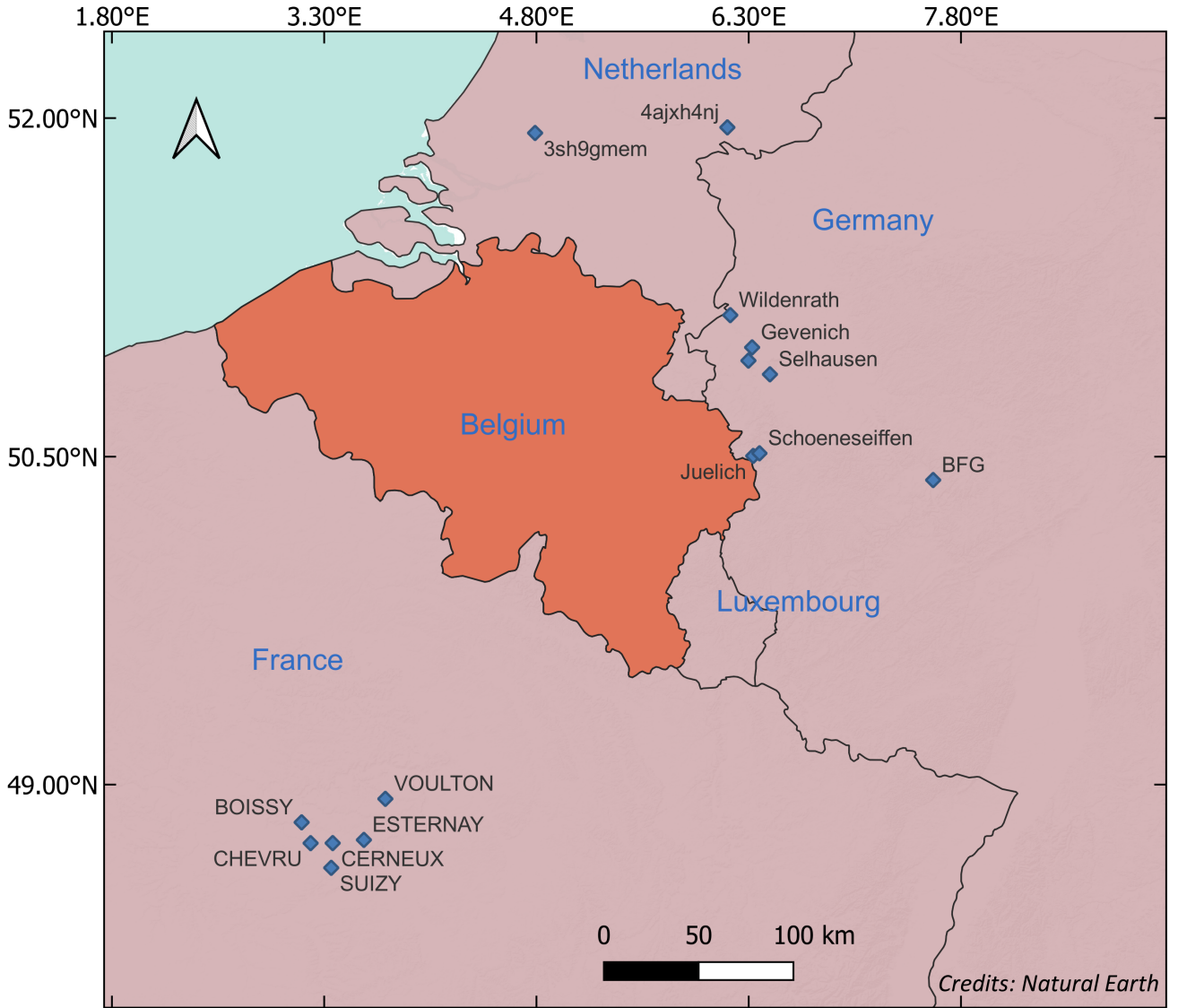


Figure 2: Locations of ISMN stations (blue diamonds) used to validate mHM soil moisture

$$f_{SM} = \frac{1}{\theta_{\text{stress-index-C1}}} \cdot \frac{\theta - \theta_{pwp}}{\theta_{sat} - \theta_{pwp}} \quad (5)$$

194 The model uses the MPR routine to compute the saturation moisture content, field capacity
 195 (θ_{fc}) and wilting point (θ_{pwp}).

196 2.2.3 Model evaluation

197 The accuracy and spatial representativeness of absolute soil moisture values are strongly source-dependent
 198 (in situ or modelled), so direct comparisons between different datasets can be misleading (Ford
 199 & Quiring, 2019; Koster et al., 2009). On one hand, simulated soil moisture is highly dependent
 200 on the quality of meteorological forcings and the physical parameterization of the model (Koster
 201 et al., 2009; Nicolai-Shaw et al., 2015; Wang et al., 2011). On the other hand, in situ measurements

are highly localized to the sensor location and are affected by the technology used by the sensor and the sufficiency of the calibration techniques (Peng et al., 2025). From a drought analysis perspective, the real information value of soil moisture is not in its absolute values but rather in its temporal variability metrics, such as anomalies and seasonal variability of soil wetness (Koster et al., 2009). This information value is generally more consistent and transferable between different sources when soil moisture is suitably normalised to have the same range and variability (Dirmeyer et al., 2004; Wang et al., 2011). Koster et al. (2009) show that if soil moisture from different sources differs only in their mean and standard deviation, then standardizing each time series (as in Equation 6) would generate nearly identical datasets of standard normal deviations (θ').

$$\theta' = \frac{\theta - \theta_m}{\sigma_m} \quad (6)$$

Where θ is the soil moisture at a given point and time of year, θ_m and σ_m are the mean and standard deviation of soil moisture, respectively, for the same point and time of year.

In our evaluation of the mHM soil moisture, we used this approach to analyze the level of temporal agreement between the standard normal deviations of mHM and in situ soil moisture from the corresponding depths at the selected ISMN stations (Figure 2).

For each in situ–modelled pair, we quantified the agreement in drought anomaly dynamics by calculating the Pearson correlation coefficient (r). To obtain an overall agreement across all sites, we first transformed the r values to the Fisher z -scale ($z = \text{arctanh}(r)$) to stabilize variance and avoid bias from the nonlinear r -scale. The z -values were then averaged to obtain \bar{z} , and finally back-transformed to yield $\bar{r} = \tanh \bar{z}$.

Prior to the comparison, we performed a quality check on the in situ data to flag and exclude potentially erroneous measurements. We considered only errors due to systematic drift in measurements over time (jumps or drops) and spiky measurements that are not explained by random noise. Here we used the quality control algorithms on in situ soil moisture developed by Dorigo et al. (2013) considering only stations that have at least 10 years of observations.

Because soil moisture is also coupled with runoff through the terrestrial water budget, we added an independent check for model simulations against daily river-discharge observations from the major river basins in Belgium. For this, we used the inbuilt calibration feature of mHM and calibrated the model using data from river gauging stations all over the country, obtained from the Waterinfo database for Flanders (<https://waterinfo.vlaanderen.be/Meetreksen>, last accessed March 2025) and the hydrometric network of discharge in Wallonia (<https://hydrometrie.wallonie.be/home/observations/debit.html?>, last accessed May 2025). In total we used 91 gauging stations during the calibration period (2000–2023) and 155 stations to validate the model from 1970–1999.

2.3 Characterizing soil moisture droughts

To characterize soil moisture droughts, we use a monthly soil moisture index (SMI), following Samaniego et al. (2013), considering the total soil water content of the root zone up to a depth of 0.5 m (We limit our analysis to this depth since groundwater in some regions is shallower than 0.5m). For each month, grid cell soil moisture is expressed as a percentile relative to that month's historical soil moisture and scaled to a range between 0 and 1.

The computation of SMI in this study is based on the methodology of Samaniego et al. (2010),

241 which proceeds as follows. Firstly, the monthly soil moisture averaged over the root-zone depth
 242 (0.5 m for this study) is extracted and used to compute a probability distribution function (PDF)
 243 $f_t(x)$ for each grid cell as;

$$f_t(x) = \frac{1}{nh} \sum_{k=1}^n K\left(\frac{x-x_k}{h}\right) \quad (7)$$

244 Where, x is the soil moisture value at which the PDF is evaluated x_1, \dots, x_k represent the
 245 simulated monthly soil moisture values for the month t over the simulation period. Note that this
 246 conversion is done for each calendar month separately to account for inherent seasonality in SM
 247 simulations. K is a Gaussian kernel function and h is the bandwidth that controls the smoothness
 248 of the kernel (equation 8). The optimal value of h is computed using a cross-validation criterion.

$$K(x, x_k) = \frac{1}{\sqrt{2\pi}h^2} \exp\left(-\frac{(x-x_k)^2}{2h^2}\right) \quad (8)$$

249 The monthly grid cell SMI is then derived by integrating $f_t(x)$ and the resulting SMI values are
 250 classified into percentiles. Drought-affected grid cells are identified using a threshold percentile
 251 τ , which is commonly set at 0.2 (e.g., Samaniego et al., 2018; Samaniego et al., 2013; Svoboda
 252 et al., 2002). This means that for a given month, a grid cell is experiencing drought if the soil
 253 moisture value falls below the 20th percentile of values for that month. According to Svoboda et al.
 254 (2002), this percentile represents the threshold at which the magnitude of drought begins to damage
 255 crops, cause water shortages and present high risks of fire. Next, adjacent cells where $SMI \leq \tau$
 256 (henceforth denoted as SMI_τ) at each timestep are consolidated to form drought clusters, which
 257 are defined by a minimum threshold area. Spatial clusters which share a minimum overlapping
 258 area at consecutive time steps are then joined to form multi-temporal clusters, each with a unique
 259 identity. For each cluster, the mean duration (months), areal extent from the onset to termination,
 260 and the total drought magnitude, which is the spatiotemporal integral of SMI_τ over the area affected,
 261 are computed. Following Samaniego et al. (2013), the magnitude of each event is computed as
 262 the space-time integral of the drought duration in months over the area under drought. This is
 263 represented mathematically as;

$$\text{TDM} = \sum_{t=t_0}^{t_1} \int_{A_t} [\tau - SMI_t(t)]_+ \quad (9)$$

264 t_0 and t_1 represent the onset and termination month of a multi-temporal drought event, A_t is the
 265 area under drought at timestep t expressed as a percent of the total domain area, and '+' means
 266 the magnitude is computed only for the positive part of the function. To avoid detecting small,
 267 isolated and short-lived dry spells as droughts, we specified a minimum threshold area of 640
 268 square kilometres (about 2% of total domain area) based on Samaniego et al. (2013) for an event
 269 to be considered as a drought, and an overlap area of the same size for two drought events at
 270 successive time steps to be considered as a single multi-temporal drought cluster.

3 Results

3.1 Model Performance Evaluation

The daily standardized anomalies of mHM-simulated soil moisture evaluated against in situ observations from the ISMN are shown in Figure 3. Of the 48 stations where in situ data was retrieved, 21 sites passed quality-control checks and were retained for validating the model outputs. The resulting comparison showed that the two datasets are highly temporally correlated, with a mean Pearson $\bar{r}=0.86$ (back-transformed averages from the Fisher z-scale), although the strength of the correlation varied with sensor depth and type. The correlation is lowest for the top 50 mm of the soil profile ($\bar{r}=0.81$ for all networks) and increases to 0.86 for the profile depths greater than 150 mm.

Even for the selected in situ sites, some still exhibited spurious spikes outside of random noise (shown by the red scatter points in Figure 3). We chose not to discard these points so as to preserve an adequate number of validation stations and to highlight the practical difficulty of obtaining perfectly reliable reference soil moisture data for validating model outputs. Despite such outliers, the model simulations and ISMN observation showed similar temporal variability in soil wetness and dryness. The difference mainly occurred in the top 50 mm layer during very dry episodes when mHM produced more extreme negative anomalies than most sensors (Figure 3 (a-d)). This explains why the correlation between the datasets is the lowest at this depth. We attribute this divergence partly to a flooring effect of capacitive sensors, which tend to plateau at very low volumetric water contents, whereas the model continues to resolve further drying. For deeper layers, the intensity and duration of dryness were more consistent between both datasets.

To evaluate how well the model simulates drought conditions, we investigated the drought-day detection skill (when the observed standardized anomaly fell below its 20th percentile) by counting hits (H ; days when both model and observations indicate drought), misses (M ; observed drought days not flagged by the model), false alarms (F ; days flagged as drought by the model but not by the observations), and correct negatives (C ; days when both indicate non-drought). (The methodology is described in more detail in Supplementary Text S1). From this analysis, we found that the model shows high skill in reproducing observed drought conditions, as it was able to detect 74% of observed drought days from the 21 stations. The false alarm rate was also only 5%, while the mean F_1 score (which summarizes the balance between misses and false alarms as $2H/(2H + F + M)$) was 75%. We attribute the differences in detecting droughts to the scale mismatch between mHM soil moisture, which represents average conditions over a grid cell, and the highly localized nature of point in situ measurements. Nevertheless, these metrics indicate that the model can be applied to study droughts.

Regarding streamflow performance, the model shows good and spatially consistent skill across the entire modelling domain and thus provides a reliable basis for analysing soil moisture dynamics. We evaluated daily discharge at 168 gauging stations. During calibration, the mean Nash-Sutcliffe Efficiency (NSE) across stations was 0.62, with 80% of stations achieving $NSE \geq 0.5$ (a commonly used benchmark for satisfactory streamflow simulation). Model performance during the validation period was also comparatively good, with a mean NSE of 0.63 and 83% of stations recording $NSE \geq 0.5$. The full details of the streamflow evaluation, including the NSE definition, are provided in Supplementary Text S2 (Figure S1).

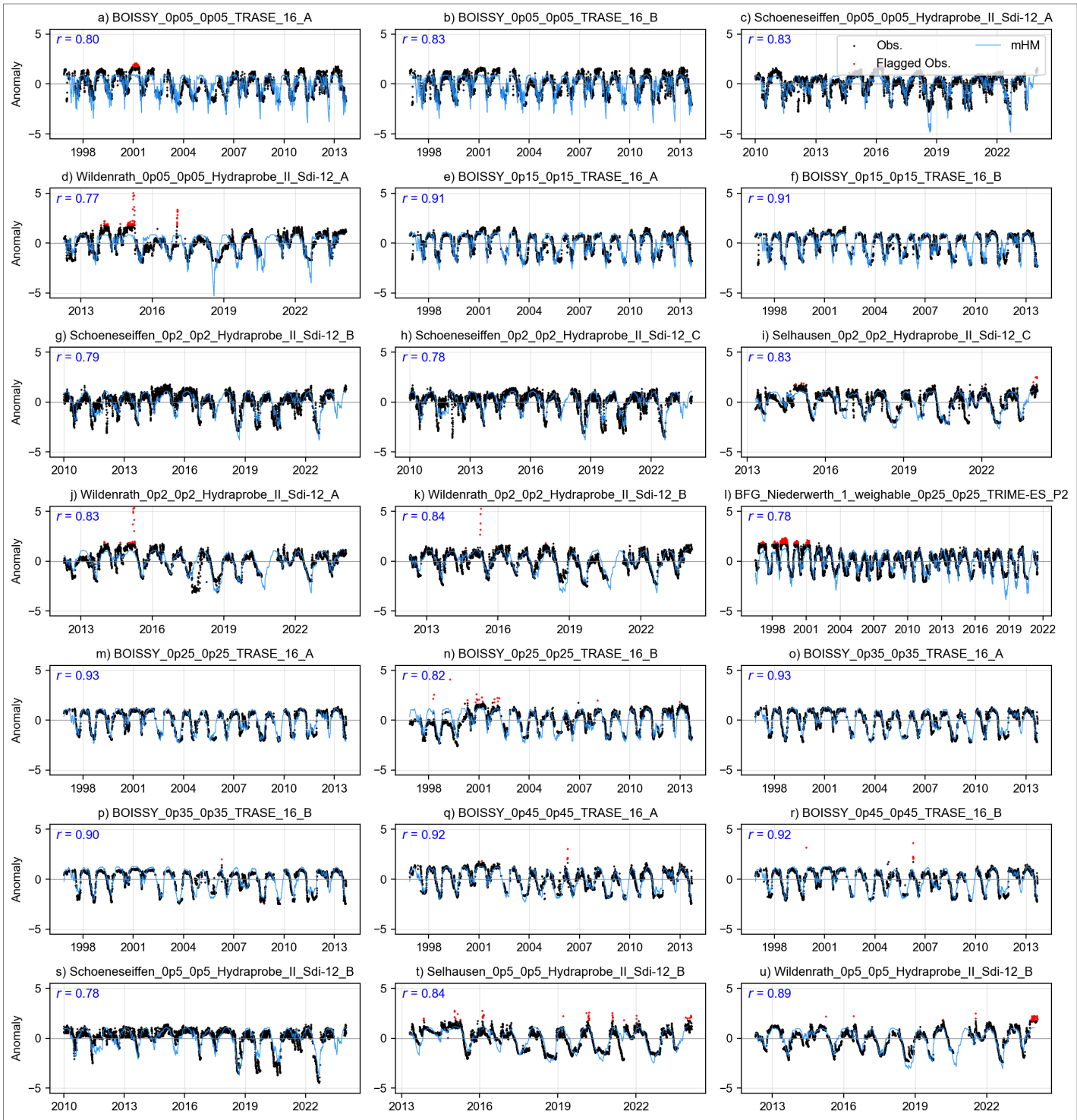


Figure 3: Comparison of standardized anomalies between mHM and in situ soil moisture at selected ISMN sites, ordered by increasing sensor depth. The red scatter points represent observed soil moisture values flagged as potentially erroneous. Titles follow the format station_topdepth_bottomdepth_sensortype, e.g., BOISSY_0p05_0p05_TRASE_16_A refers to the Boissy station with a sensor at 0.05 m depth and sensor type TRASE.

3.2 Decadal evolution of soil-moisture droughts

To summarize how soil-moisture drought behaviour evolves across decades, we use three complementary metrics. First, we quantify the magnitude of each event using the Total Drought Magnitude

(TDM), which integrates drought severity over space and time and thus allows drought events to be ranked consistently (Section 3.2.1). Second, in Section 3.2.2, we describe how drought severity is distributed by quantifying the fraction of drought-affected area falling into different severity classes (moderate, severe, extreme, and exceptional) within each decade. These classes capture shifts in the composition of drought conditions beyond just the total magnitude. Third, in Section 3.2.3, we quantify cumulative drought exposure as the total number of months in which each grid cell experiences drought per decade (months need not be consecutive). This metric summarizes how frequently drought conditions recur at a given location over a decade. For decadal summaries, we defined decades starting from 1971 (i.e., 1971–1980, 1981–1990, ...) since SPEI construction requires accumulated water-balance anomalies over preceding months (January 1970 will thus not have SPEI-1 values, while January–March 1970 lacks SPEI-3 values. The first year with complete SPEI values is 1971).

3.2.1 Magnitude-based ranking of soil-moisture drought events

Figure 4 shows the magnitude of simulated soil moisture droughts in Belgium between 1970 and 2020 based on the Total Drought Magnitude (TDM), the cumulative deficit in soil moisture below the drought threshold ($SMI \leq 0.20$), integrated over the affected area and the event duration. To ensure an unambiguous severity ranking, the events are ranked by TDM and when two events have similar TDM (difference $< 1\%$), ranks are resolved using a fixed tie-breaker hierarchy: (i) average drought area (fraction of the domain with $SMI \leq 0.20$ averaged over the entire event), (ii) duration, and (iii) exceptional-class exposure (fraction of $SMI \leq 0.020$ summed over the duration of the event). On the basis of this ranking, Table 2 displays the corresponding metrics for the ten largest droughts during the period of analysis. From an interdecadal perspective, Figure 4 reveals three distinct drought regimes. Beginning with the 1970s, three major drought events are apparent, dominated by the historic 1975–1977 drought. Although this event is commonly referred to as the 1976 drought, probably because that is when it peaked, the analysis shows that its development in Belgium began back in the autumn of 1975 and lasted for a record 16 months until the winter of 1977. By the end of the event, almost 63% of the domain had experienced drought conditions, although this fluctuated over time². This event established a benchmark against which subsequent droughts in many parts of Europe are commonly compared. Our analysis reflects this, as this event almost matches the most intense drought in Belgium during the period of our analysis.

The subsequent three decades (1981–1990, 1991–2000, and 2001–2010) are characterized by a comparatively wetter hydroclimatic regime, reflected in the lower-magnitude drought events in Figure 4. Only three events from this period appear in the top ten, and all rank relatively low by TDM. The largest of these, the 1995–1996 drought, nonetheless persisted for 13 months.

A significant shift in drought frequency and severity emerged after 2011. Of the ten biggest droughts from 1971, four of them were recorded between 2011 and 2020, three of which occurred in rapid succession between 2016 and 2020. The 2016–2017 drought is the biggest in this period, exceeding even the 1975–1977 drought by TDM and affected area (64%) and lasting nearly as long (15 months), as shown in Table 2. The 2018–2019 drought also ranks among the largest events, exceeded in TDM only by the 2016–2017 and 1975–1977 droughts (Table 2). Although it persisted

²63% is the mean fraction of the domain affected across all time steps during the drought; at individual times coverage ranged below and above this value, with a maximum of complete (100%) coverage when the drought peaked

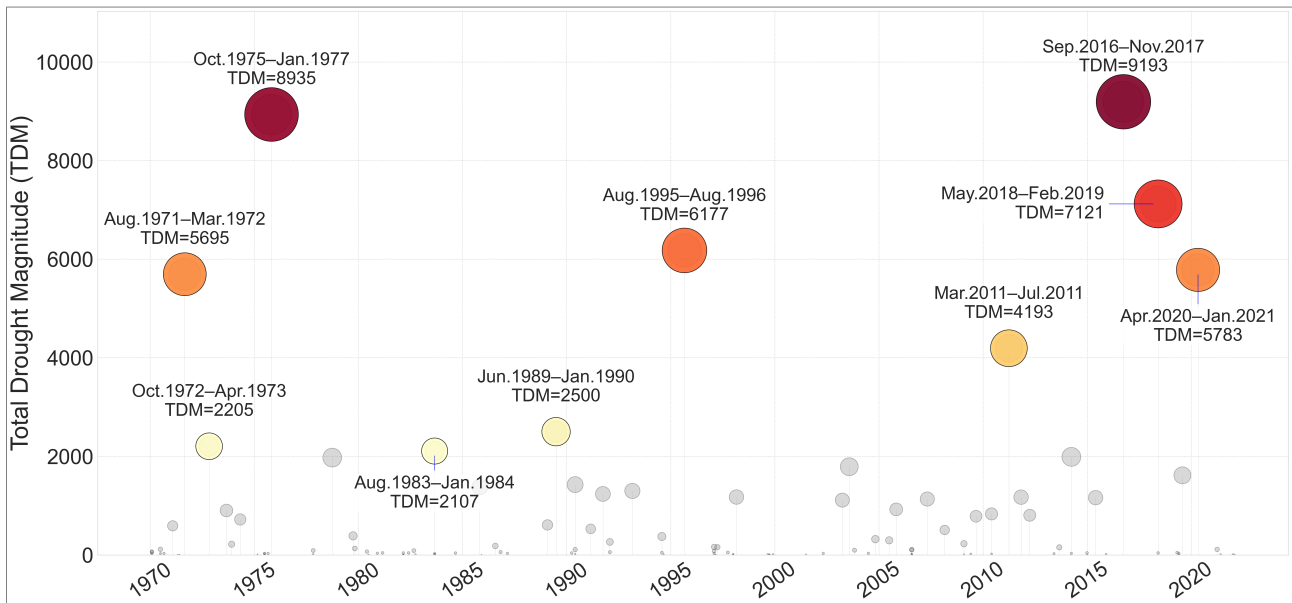


Figure 4: Duration and magnitude of drought events from 1970 to 2020. Each circle represents a drought event, positioned according to its start date (x-axis). The circle size is proportional to the Total Drought Magnitude (TDM) of each event. The ten most severe droughts, ranked by TDM, are highlighted with coloured markers, with their corresponding periods annotated. Events are ranked primarily by TDM; when two events have similar TDM (difference $\leq 1\%$), ranks are determined by peak affected area, then duration, then exceptional-class exposure (defined as $SMI \leq 0.02$).

356 for only 10 months, it affected a large fraction of the domain on average (73%). Although some
 357 big droughts have occurred after 2020, we have excluded these from our inter-decadal analysis
 358 because the current decade is still incomplete.

3.2.2 Decadal shifts in drought severity

359 While TDM provides a suitable event-ranking metric, it aggregates drought conditions over space
 360 and time and therefore does not directly indicate whether severity arises from widespread moderate
 361 drought or short periods of extreme conditions. To resolve this, we classified all the drought events
 362 into four severity classes following Svoboda et al. (2002): moderate drought ($0.1 < SMI \leq 0.2$),
 363 severe drought ($0.05 < SMI \leq 0.1$), extreme drought ($0.02 < SMI \leq 0.05$), and exceptional drought
 364 ($SMI \leq 0.02$). We then examined how the severity of droughts has evolved within and across
 365 decades, as shown in Figure 5. For conciseness we will examine the changes at both ends of the
 366 drought severity spectrum.
 367

368 As Figure 5 shows, droughts during 1971–1980 were predominantly moderate ($0.1 < SMI$
 369 ≤ 0.2). When exceptional droughts occurred, they remained spatially limited, peaking at below
 370 30% of the domain during the 1971–1972 and 1975–1977 events (shown by the black dots in
 371 Figure 5). As the figure shows, these two droughts were disrupted by wetter spells, which allowed
 372 the re-establishment of normal to wet soil moisture conditions between drought phases. When
 373 accumulated over the decade, moderate droughts accounted for almost 75% of all grid-cell months
 374 affected by drought, whereas exceptional drought contributed $\sim 3\%$, largely associated with the
 375 1975–1977 event (donut plots in Figure 5).
 376

Between 1981 and 2010, the drought regime was characterized by predominantly normal-to-

Table 2: The ten biggest soil moisture drought events in Belgium, ranked by Total Drought Magnitude (TDM).

Rank	Event period	TDM	Average af- fected area (%)	Duration (months)	Exceptional class exposure (%·mo)
1	Sep 2016–Nov 2017	9193	64.0	15	182.9
2	Oct 1975–Jan 1977	8935	62.6	16	103.4
3	May 2018–Feb 2019	7122	73.1	10	108.3
4	Aug 1995–Aug 1996	6177	60.3	13	69.8
5	Apr 2020–Jan 2021	5783	58.0	10	27.7
6	Aug 1971–Mar 1972	5695	72.9	8	57.3
7	Mar 2011–Jul 2011	4193	81.6	5	84.9
8	Jun 1989–Jan 1990	2500	51.5	8	8.0
9	Oct 1972–Apr 1973	2205	35.4	7	11.2
10	Aug 1983–Jan 1984	2107	47.0	6	22.4

377 wet conditions interspersed with episodic, short-lived droughts. Decadal aggregates indicate that
378 at least 80% of drought-affected grid-cell months during this period were moderate in intensity,
379 whereas exceptional drought contributed on average less than 1% (Figure 6). However, individual
380 events (e.g., the 1995–1996 drought) still exhibited brief peaks of exceptional drought extent when
381 exceptional conditions reached ~30% of the domain (Figure 5).

382 By contrast, the 2011–2020 period experienced more frequent and severe droughts, particularly
383 towards the end of the decade (Figure 5). In comparison to the previous decades, the spatial footprint
384 of exceptional droughts noticeably increased. At the peak of the 2011 droughts, exceptional
385 droughts affected close to 70% of the domain, while during the 2016–2017 drought, about 40%
386 of the drought-affected area was under exceptional drought, which did not previously occur even
387 during the 1975–1977 event. This increase is reflected in the decadal drought area severity, where
388 exceptional droughts accounted for 5.9% of drought-affected area, a proportion that exceeds all the
389 previous four decades combined (Figure 5).

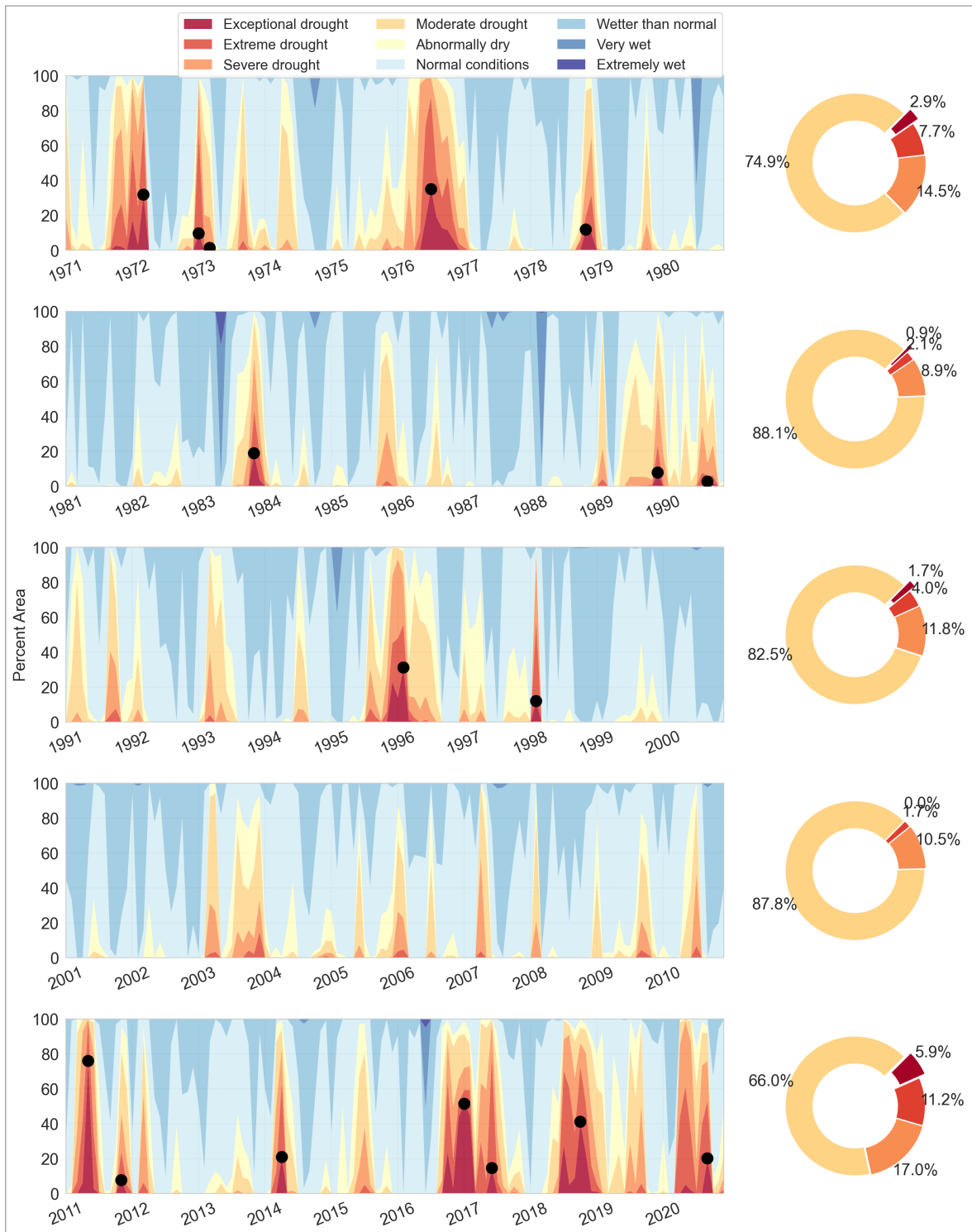


Figure 5: Decadal evolution of drought severity in Belgium, 1971–2020. The stacked panels (left) show the monthly percentage of land area in each soil-moisture class. Black dots mark the peak extent of exceptional drought ($SMI \leq 0.02$). The donut charts (right) summarize, for drought months only ($SMI \leq 0.20$), the mean share of drought-affected area in each drought class; months without drought contribute no area.

3.2.3 Decadal drought exposure

Complementing the temporal and spatial analyses, Figure 6 illustrates decadal cumulative drought exposure, expressed as the total number of months in which each grid cell experienced $\text{SMI} \leq 0.2$ in a decade. During 1971–1980, the domain accumulated between 12 and 36 drought months, with a domain-wide mean of about 24 months per grid cell (2.4 months/year) (Figure 6 inset histogram). Domain-wide improvements in moisture conditions are apparent in the next three decades. The mean cumulative totals fell to 13 months in 1981–1990 (1.3 months/yr), 17 months in 1991–2000 (1.7 months/yr.), and 14 months in 2001–2010 (1.4 months/yr). As with the other metrics, cumulative drought exposure peaked in 2011–2020. The domain accumulated between 24 and 48 months of drought over the decade, and the domain-wide mean rose to 37 months, or 3.7 months per year (Figure 6). To put this into perspective, this amounts to roughly three continuous years of soil-moisture drought within the decade. This cumulative exposure is more than twice that of each of the three preceding decades (1981–1990, 1991–2000, 2001–2010) and about 1.5 times higher than the previous driest decade, 1971–1980.

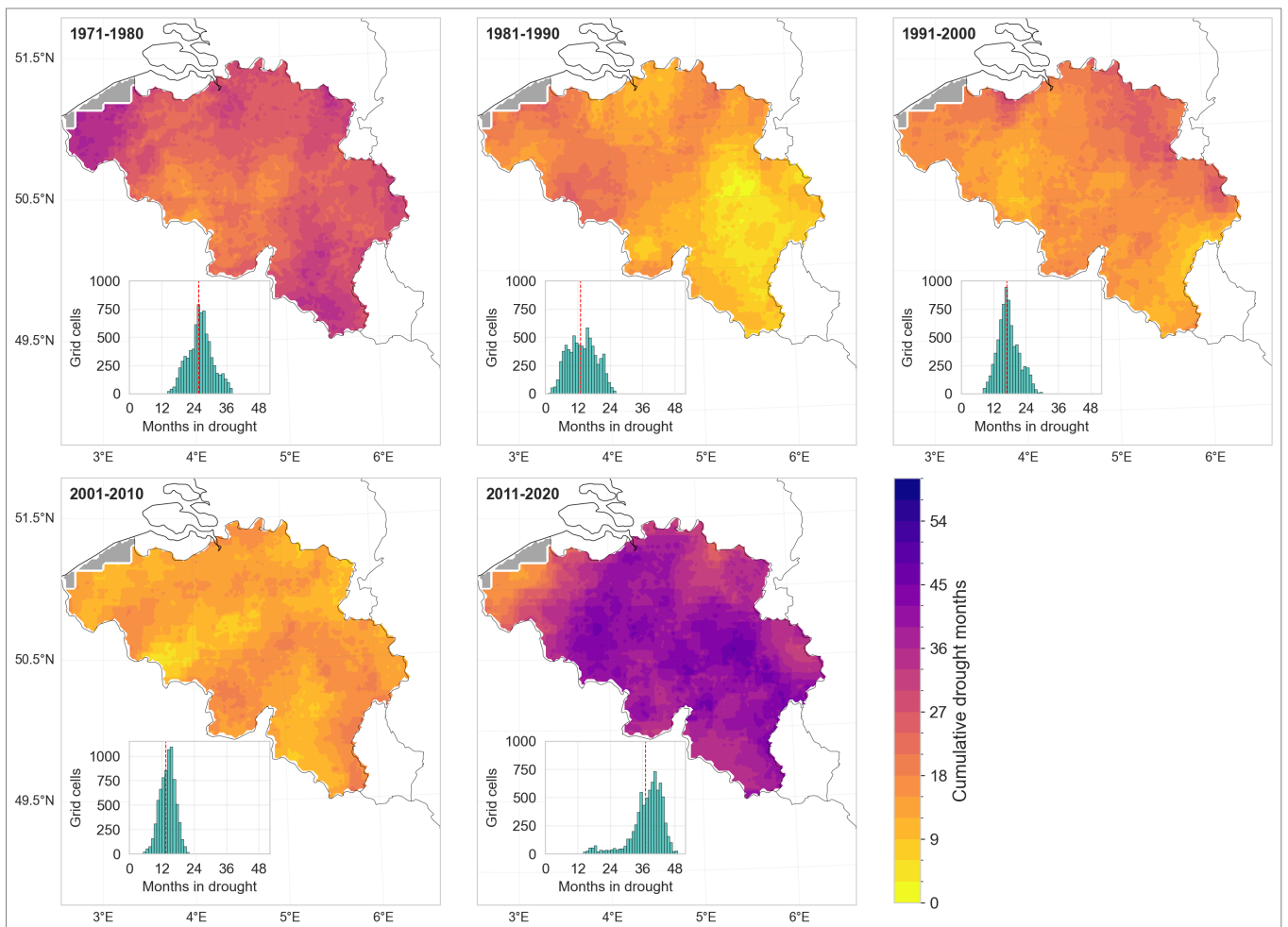


Figure 6: Cumulative decadal drought exposure expressed as the number of months within each decade that a grid cell experienced drought conditions ($\text{SMI} \leq 0.2$). The inset histograms show the frequency distribution of cumulative time under drought for all grid cells. The red dashed line indicates the mean duration. EOBS data is missing for the region shaded grey.

To test whether 2011–2020 was statistically drier than the preceding four decades, we applied

a non-parametric bootstrap to the per-pixel cumulative drought durations ($\text{SMI} \leq 0.20$) and to the subset of exceptional drought months ($\text{SMI} \leq 0.02$). For each decade, we generated 100,000 bootstrap samples by resampling grid-cell drought durations with replacement, calculated the mean for each sample, and used the 2.5th and 97.5th percentiles of the resulting distribution to derive the 95% confidence interval (CI) of the sample mean.

The statistical analysis concludes that 2011–2020 was indeed the driest decade of the five decades, both in terms of total drought duration and exposure to exceptional droughts. Over the decade, Belgium accumulated a mean drought period of 37 months (CI: 36.9–37.2 months), significantly higher than in 1971–1980 (mean=25.65 months [CI: 25.6–25.8]), which is the next driest decade (Figure 7 (a)). The lower bound of the 2011–2020 decade CI lies 11 months above the upper bound of the 1971–1980 period and far higher than those experienced in the three decades in between (1981–1990: mean 13 months [CI: 12.92–13.15], 1991–2000: mean 16.9 months [CI: 16.80–16.95] and 2001–2010: mean 13.52 months [CI: 13.46–13.59]).

A similar contrast emerges for the most severe drought (Figure 7(b)). The 2011–2020 decade accumulated 4.3 months of exceptional drought on average (CI: 4.28–4.38), more than the combined total of the four earlier decades. None of the previous decades reached a mean of 2 months of exceptional droughts. 1971–1980 accumulated 1.94 months (CI: 1.89–1.98), 1981–1990 only 0.35 months (CI: 0.34–0.36), 1991–2000 0.80 months (CI: 0.79–0.84), and 2001–2010 experienced virtually no exceptional drought. In cumulative terms, more than half of all exceptional drought months in the five-decade record occurred between 2011 and 2020.

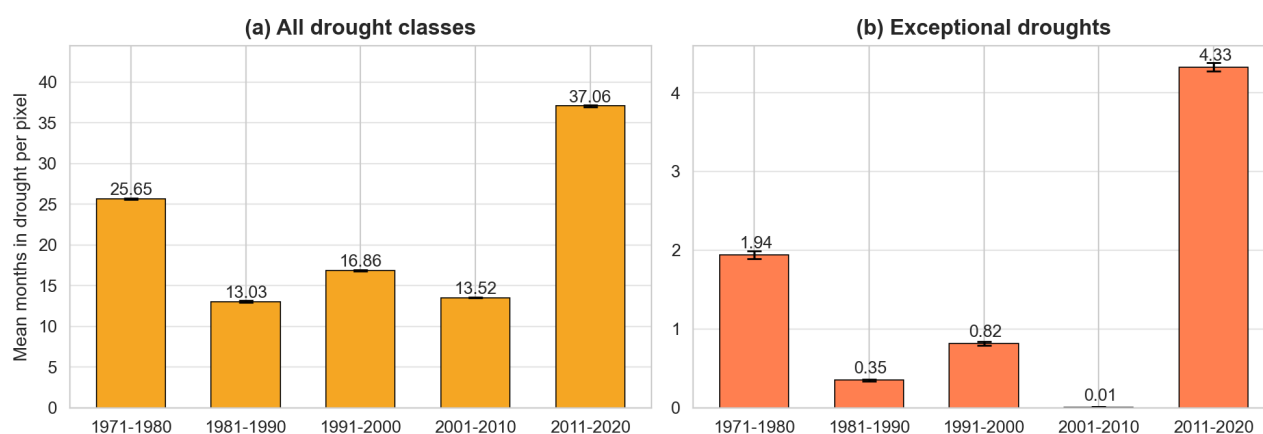


Figure 7: Decadal pixel-wise cumulative drought exposure. The bars show the mean number of months each grid cell spent in drought per decade (not necessarily consecutive), with 95% bootstrap confidence intervals (black whiskers) for (a) All drought classes ($\text{SMI} \leq 0.20$) and, (b) exceptional drought only ($\text{SMI} \leq 0.02$).

3.3 Divergence between soil moisture and SPEI droughts

To examine how precipitation-based drought indicators reflect land-surface moisture stress, we compared SMI and SPEI patterns during the three most severe soil moisture drought events ranked by total drought months (TDM): 1975–1977, 2016–2017, and 2018–2019. Because SMI is computed on a monthly timescale, we derived the climatic water balance (precipitation minus potential evapotranspiration) from E-OBS and calculated SPEI at one- and three-month

431 accumulation periods. Pixel-wise SPEI-1 and SPEI-3 were computed using the SPEI package
432 developed by Vonk (2024). We limited the accumulation period to three months because this
433 timescale is currently used in operational drought monitoring in Belgium. Since SPEI is anomaly-
434 based rather than percentile-based, we associated $\text{SPEI} = -1.0$ with $\text{SMI} = 0.2$ to represent the
435 threshold for at least moderate drought, following the drought severity guidelines of Svoboda
436 et al. (2002). We evaluated the differences between indices in terms of (i) anomaly magnitude, (ii)
437 drought persistence (maximum number of *consecutive* months under at least moderate drought
438 within an event), and (iii) cumulative drought exposure (total number of months, not necessarily
439 consecutive, under at least moderate drought within the event window).

440 In terms of anomaly magnitude, SMI generally indicated stronger and longer-lasting deficits
441 than SPEI-1 and, to a lesser extent, SPEI-3 (Figure 8). SPEI-1 responds strongly to short-lived
442 precipitation anomalies that may not immediately translate into changes in root-zone storage. By
443 design, SPEI-3 smooths some of the short-term variability in SPEI-1 and more closely resembles
444 the temporal evolution of soil-moisture anomalies, but still tends to underestimate deficit magnitude
445 relative to SMI over our domain (Figure 8). Among the three events, SMI indicated the strongest
446 soil moisture deficits during 2016–2017 (with SMI approaching zero), which is not reflected in
447 either SPEI-1 or SPEI-3. Although the 2016–2017 drought was interrupted by intermediate wet
448 conditions during March and April 2017, leading to partial recovery, this wet spell did not split the
449 event because the month-to-month overlap in drought area remained above the 640 km² merging
450 threshold, and the drought therefore remained a single multi-temporal event.

451 We also found that SMI-based droughts exhibited higher persistence than SPEI-based droughts.
452 Median persistence for SMI was 9 months in 1975–1977, 6 months in 2016–2017, and 7 months in
453 2018–2019 (Table 3). In comparison, SPEI-1 shows much shorter median persistence (3 months in
454 1975–1977 and 2 months in both 2016–2017 and 2018–2019), while SPEI-3 is closer to SMI but
455 remains lower (7 months in 1975–1977 and 5 months in both 2016–2017 and 2018–2019).

456 The same pattern is evident for cumulative drought exposure. Median cumulative exposure
457 for SMI was 10 months in 1975–1977 and 2016–2017 and 8 months in 2018–2019, compared
458 with 4, 6, and 3 months for SPEI-1 and 7, 8, and 6 months for SPEI-3 (Table 3, additional maps in
459 Supplementary Text S3, Figures S3 and S4).

460 This systematically longer persistence and exposure shown by the SMI indicates that soil
461 moisture droughts last longer than precipitation-based droughts because transient precipitation
462 events do not necessarily translate into root-zone recovery. Additional description on the patterns
463 of SMI and SPEI recovery is presented in Supplementary Text S3.

464 The differences presented herein do not imply that one indicator is necessarily *better*; rather,
465 they are all useful for demonstrating how a drought shock progressively propagates through
466 different components of the hydrological system. Precipitation-based indices like SPEI reflect
467 short-term meteorological inputs that may still be agriculturally meaningful. As Figure 8 shows,
468 rainfall events during dry periods may not replenish deeper soil moisture due to immediate losses
469 through evapotranspiration, yet these events can still temporarily alleviate plant water stress,
470 especially for fast-responding, shallow-rooted crops or annual crops. The recovery of SPEI out of
471 drought conditions may thus signal 'relief' that is real, albeit short-lived and limited in scope. On
472 the other hand, SMI-based drought analysis better captures the persistence of land surface water
473 deficits and the residual moisture stresses that continue to affect the dependent ecosystems (e.g.,

perennial deep-rooted vegetation) long after meteorological conditions have normalized.

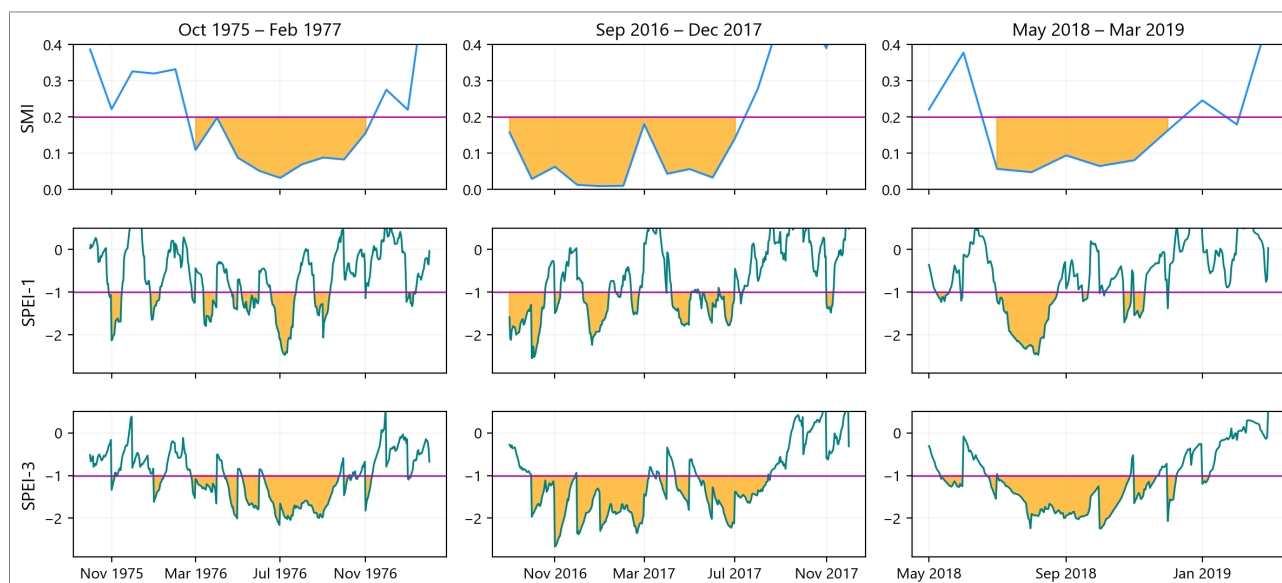


Figure 8: Comparison of domain-average SMI, SPEI-1, and SPEI-3 time series during the three biggest drought events up to 2020. The orange shaded areas indicate drought conditions, defined as $SMI \leq 0.2$ and $SPEI \leq -1.0$. The horizontal magenta lines mark the drought threshold for each index.

Table 3: Domain-wide median persistence and cumulative drought exposure for the events in Fig. 8, based on SMI, SPEI-1, and SPEI-3.

Index	Max. consecutive months (persistence)			Total drought months (cumulative exposure) ^a		
	1975-1977	2016-2017	2018-2019	1975-1977	2016-2017	2018-2019
SMI	9	6	7	10 (16)	10 (15)	8 (10)
SPEI-1	3	2	2	4 (7)	6 (8)	3 (5)
SPEI-3	7	5	5	7 (13)	8 (12)	6 (9)

^a Values in parentheses denote the maximum cumulative exposure until all pixels emerge out of drought.

4 Discussion

This extended temporal analysis of soil moisture droughts over Belgium offers new insights on the severity of recent droughts in the country. Using multiple drought metrics, we show that droughts in the 2010s were substantially more frequent and severe than in the preceding four decades since 1970. Our findings fit into the wider pan-European narrative of intensifying droughts over the continent in the 21st century. García-Herrera et al. (2019) showed that the 2016–2017 drought in central-western Europe was among the most severe events in the recent observational record. Longer-term reconstructions further indicate that the succession of European summer droughts between 2015 and 2018 was exceptional even in a millennial context (over the previous 2,110 years) (Büntgen et al., 2021; Hari et al., 2020; Rakovec et al., 2022). This recent intensification of droughts has been attributed to a combination of persistent atmospheric blocking and anthropogenic warming, which together reduce moisture supply and enhance evapotranspiration (García-Herrera

487 et al., 2019; Hari et al., 2020; Ionita et al., 2020). Under continued warming, these conditions are
488 projected to increase the frequency and severity of similar magnitude droughts (Hari et al., 2020;
489 Rakovec et al., 2022; Samaniego et al., 2018).

490 On the comparison between precipitation and soil-based drought indicators, we stress that these
491 indicators are useful for different components of the hydrological system. SPEI-1 and SPEI-3 may
492 suit analyzing drought patterns in shallow soil layers and shorter temporal scales but are limited for
493 indicating drought persistence deeper in the soil or in complex ecosystems due to their ignorance of
494 land-ecosystem interactions (Peng et al., 2024; Xu et al., 2021). When assessing drought impacts
495 on ecosystems, groundwater recharge, or perennial vegetation like forests, the divergence between
496 meteorological and soil moisture signals can become complex. In such systems, soil properties such
497 as hydrophobicity during prolonged dry periods can lead to highly uneven infiltration (Filipović
498 et al., 2018; Gimbel et al., 2016). Heavy summer rainfall may not be absorbed uniformly across
499 the soil profile but instead run off or infiltrate preferentially along cracks, roots, or macropores,
500 sometimes bypassing the upper root zone. While this limits the ability of standard soil moisture
501 indices to reflect actual water availability near the surface, it may still benefit deep-rooted vegetation
502 like trees by replenishing deeper soil layers (Duniway et al., 2018; Zhu et al., 2015). Assessing
503 drought stress and recovery in these systems thus requires models and indicators that account for
504 vertical and spatial heterogeneity in infiltration and root water uptake (e.g., Shen et al., 2025),
505 rather than relying solely on averaged or surface-weighted soil moisture metrics. Further, while it
506 may be argued that SPEI at longer accumulation periods (e.g., 6, 9 or 12 months) can lead to a
507 closer resemblance of root-zone moisture conditions, finding the appropriate accumulation lengths
508 is dependent on landscape and soil characteristics (topography, rooting depth, soil hydrology and
509 management conditions) and climatic conditions, which can lead to a strong variation of drought
510 characteristics if the landscape is heterogeneous. Kumar et al. (2016) indeed found that applying
511 spatially variable accumulation periods achieves a higher correlation between precipitation-based
512 and groundwater drought indices over a uniform domain-wide accumulation period, even at long
513 accumulation times.

514 Our findings are relevant beyond Belgium because the workflow used in this study can be
515 transferred to other regions provided that the meteorological forcing is available at appropriate
516 resolution, a hydrological or land-surface model is parameterized to represent soil-water storage,
517 and consistent long-term simulations can be produced. Extending the analysis to other domains
518 would allow the same drought dynamics addressed in this study to be evaluated under different
519 climate gradients, soil, land-cover conditions, and management regimes.

520 From an operational perspective, the results support a monitoring strategy that complements
521 precipitation-based indices with soil-moisture-based indicators rather than interchanging them. As
522 we have shown, precipitation-based indices are useful for tracking meteorological anomalies and
523 can provide early signals of emerging drought risk, but they may not capture persistent impacts
524 when land-surface memory sustains root-zone deficits after rainfall resumes. In an operational
525 system, precipitation-based indices can be used for early warning, while a root-zone soil moisture
526 drought indicator is better utilized to track agricultural drought development and recovery and to
527 assess when conditions have returned to normal in the soil profile. These outputs can be integrated
528 into management decisions by linking drought phase and persistence to sector-relevant decisions.
529 For example, soil-moisture drought persistence is directly relevant for agricultural advisories that

530 inform planting and irrigation planning and signaling crop yield risk and the risks associated
531 with the occurrence of wildfires or floods that can occur due to seasonally saturated soils. Slow
532 recovery in soil and catchment storage after meteorological drought can also inform water supply
533 preparedness and groundwater management, since water resources often show a delayed return to
534 normal conditions (Yang et al., 2017). For inland navigation and low-flow management, combining
535 soil moisture drought information with streamflow indicators can help distinguish short, transient
536 precipitation deficits from longer-lasting, storage-driven drought conditions. In practice, monthly
537 updates of a root-zone soil moisture drought map, paired with precipitation-based indices, would
538 support earlier identification of drought evolution and lead to more realistic expectations for
539 recovery following intermittent wet periods (Van Loon et al., 2024).

540 **5 Limitations and future work**

541 Our results rely on the evaluation of model-derived soil moisture conditions, which are inevitably
542 constrained by structural, parametric, and forcing uncertainties that we did not explicitly evaluate.
543 Choices of the mapping between drought categories (e.g., SPEI = -1.0 vs. $SMI \leq 0.2$) and a
544 uniform accumulation period over the whole domain (for SPEI analysis) also introduce additional
545 subjectivity. The mHM model also does not account for anthropogenic factors such as irrigation,
546 groundwater abstraction, tile drainage and artificial canals, and land management conditions,
547 which affect the hydrology of the domain. Future work can partially offset these limitations by
548 quantifying uncertainty using ensembles of forcings, investigating model parameters to derive
549 confidence intervals for drought magnitude, area, and timing, incorporating human water use and
550 irrigation processes, or assimilating independent observations (such as in situ or remotely sensed
551 soil moisture and terrestrial water storage) to better constrain states and evaluate the joint behaviour
552 of multiple drought indicators alongside observed impacts.

553 **6 Conclusion**

554 This study provides a multi-decadal, high-resolution reconstruction of root-zone soil moisture
555 droughts over Belgium for 1970–2020. Using event-based severity metrics that quantify drought
556 duration, spatial extent, and intensity, we show that 2011–2020 was marked by substantially greater
557 cumulative drought exposure than any preceding decade, exceeding the previous driest decade by
558 about 1.5 times. The 2011–2020 decade also exhibited the highest share of exceptional drought,
559 with cumulative exceptional drought exposure exceeding that of all earlier decades combined.

560 By comparing soil-moisture drought (SMI) with precipitation-based indicators (SPEI-1 and
561 SPEI-3) for the three most severe events, we show that precipitation-based indices systematically
562 underestimate drought persistence and cumulative exposure relative to root-zone soil moisture.
563 In particular, soil moisture droughts persist longer and recover more slowly than meteorological
564 anomalies, reflecting land-surface memory. Including soil moisture monitoring in drought observa-
565 tories thus offers the added value of capturing lingering stresses on agriculture and ecosystems,
566 which can persist long after meteorological conditions have normalized. This provides decision-
567 makers with a more complete view of drought severity and duration and supports targeted response
568 and mitigation efforts.

569 The reconstructed drought record and event-based metrics presented in this study provide a
570 consistent basis for benchmarking recent droughts against historical variability and for supporting
571 drought monitoring and management.

572

Author Contributions:

573

574

575

576

KL, RK and OR formulated the study and set up the model simulations. AvG supervised the project. KL analyzed the data and wrote the first draft of the manuscript, with all authors commenting on previous versions of the manuscript. All authors read and approved the contents of the final manuscript.

577

Acknowledgements:

578

579

580

581

582

583

584

We acknowledge the work of Jens Wilhelmi (BFG_Nw network) for providing data in support of the International Soil Moisture Network. We also acknowledge the work of Arnaud Blanchouin and ORACLE team of the Institut national de recherche en sciences et technologies pour l'environnement et l'agriculture, France in support of the ISMN. We are grateful to the High Performance Computing system of Vrije Universiteit Brussel for providing the computational resources required to run the model and the analysis of model outputs. We also acknowledge all the sources of data used in this study for providing the data openly.

585

Funding:

586

587

588

589

590

KL acknowledges the financial support of the Research Foundation – Flanders (FWO) for funding the International Coordination Action (ICA) “Open Water Network: Impacts of Global Change on Water Quality” (project code G0ADS24N). OR acknowledges the Research Excellence in Environmental Sciences (REES) project of the Faculty of Environmental Sciences, Czech University of Life Sciences Prague.

591

Data Availability:

592

All datasets used in this paper are openly available as described in the methodology text.

593

Code Availability:

594

595

596

597

The scripts used to arrive at the findings of this study are available at:
https://github.com/klekarkar/pre_post_process_mHM.
The SMI analysis was carried out using the SMI package, available at:
<https://github.com/mhm-ufz/SMI>.

598

Competing interests:

599

600

At least one of the (co-)authors is a member of the editorial board of Hydrology and Earth System Sciences.

References

- Banjara, P., Shrestha, P. K., Pandey, V. P., Sah, M., & Panday, P. (2025). Quantifying agricultural drought in the Koshi River basin through soil moisture simulation. *Journal of Hydrology: Regional Studies*, *57*, 102132. <https://doi.org/10.1016/j.ejrh.2024.102132>
- Beck, H. E., McVicar, T. R., Vergopolan, N., Berg, A., Lutsko, N. J., Dufour, A., Zeng, Z., Jiang, X., Van Dijk, A. I. J. M., & Miralles, D. G. (2023). High-resolution (1 km) Köppen-Geiger maps for 1901–2099 based on constrained CMIP6 projections. *Scientific Data*, *10*(1), 724. <https://doi.org/10.1038/s41597-023-02549-6>
- Beckers, V., Beckers, J., Vanmaercke, M., Van Hecke, E., Van Rompaey, A., & Dendoncker, N. (2018). Modelling Farm Growth and Its Impact on Agricultural Land Use: A Country Scale Application of an Agent-Based Model. *Land*, *7*(3), 109. <https://doi.org/10.3390/land7030109>
- Beckers, V., Poelmans, L., Van Rompaey, A., & Dendoncker, N. (2020). The impact of urbanization on agricultural dynamics: A case study in Belgium. *Journal of Land Use Science*, *15*(5), 626–643. <https://doi.org/10.1080/1747423X.2020.1769211>
- Boeing, F., Rakovec, O., Kumar, R., Samaniego, L., Schrön, M., Hildebrandt, A., Rebmann, C., Thober, S., Müller, S., Zacharias, S., Bogen, H., Schneider, K., Kiese, R., Attinger, S., & Marx, A. (2022). High-resolution drought simulations and comparison to soil moisture observations in Germany. *Hydrology and Earth System Sciences*, *26*(19), 5137–5161. <https://doi.org/10.5194/hess-26-5137-2022>
- Bogen, H., Montzka, C., Huisman, J., Graf, A., Schmidt, M., Stockinger, M., Von Hebel, C., Hendricks-Franssen, H., Van Der Kruk, J., Tappe, W., Lücke, A., Baatz, R., Bol, R., Groh, J., Pütz, T., Jakobi, J., Kunkel, R., Sorg, J., & Vereecken, H. (2018). The TERENO-Rur Hydrological Observatory: A Multiscale Multi-Compartment Research Platform for the Advancement of Hydrological Science. *Vadose Zone Journal*, *17*(1), 1–22. <https://doi.org/10.2136/vzj2018.03.0055>
- Bonan, G. B., & Stillwell-Soller, L. M. (1998). Soil water and the persistence of floods and droughts in the Mississippi River Basin. *Water Resources Research*, *34*(10), 2693–2701. <https://doi.org/10.1029/98WR02073>
- Brisson, E., Demuzere, M., Kwakernaak, B., & Van Lipzig, N. P. M. (2011). Relations between atmospheric circulation and precipitation in Belgium. *Meteorology and Atmospheric Physics*, *111*(1), 27–39. <https://doi.org/10.1007/s00703-010-0103-y>
- Büntgen, U., Urban, O., Krusic, P. J., Rybníček, M., Kolář, T., Kyncl, T., Ač, A., Koňasová, E., Čáslavský, J., Esper, J., Wagner, S., Saurer, M., Tegel, W., Dobrovolný, P., Cherubini, P., Reinig, F., & Trnka, M. (2021). Recent European drought extremes beyond Common Era background variability. *Nature Geoscience*, *14*(4), 190–196. <https://doi.org/10.1038/s41561-021-00698-0>
- Cao, S., Li, M., Zhu, Z., Wang, Z., Zha, J., Zhao, W., Duanmu, Z., Chen, J., Zheng, Y., Chen, Y., et al. (2023). Spatiotemporally consistent global dataset of the gimms

641 leaf area index (gimms lai4g) from 1982 to 2020. *Earth System Science Data*,
642 15(11), 4877–4899. <https://doi.org/10.5194/essd-15-4877-2023>

643 Cornes, R. C., Van Der Schrier, G., Van Den Besselaar, E. J., & Jones, P. D. (2018). An
644 ensemble version of the E-OBS temperature and precipitation data sets. *Journal*
645 *of Geophysical Research: Atmospheres*, 123(17), 9391–9409. [https://doi.org/10.](https://doi.org/10.1029/2017JD028200)
646 [1029/2017JD028200](https://doi.org/10.1029/2017JD028200)

647 De Ridder, K., Coudere, K., Depoorter, M., Liekens, I., Pourria, X., Steinmetz, D.,
648 Vanuytrecht, E., Verhaegen, K., & Wouters, H. (2020). *Evaluation of the socio-*
649 *economic impact of climate change in belgium* (Summary for Policymakers) (Study
650 commissioned by the National Climate Commission). National Climate Commis-
651 sion. <https://climat.be/doc/seclim-be-2020-spm-en.pdf>

652 De Vlaamse Waterweg nv. (2022). *Economische schade van droogte voor de binnenvaart*
653 *in Vlaanderen*. De Vlaamse Waterweg nv. [https://www.vlaamsewaterweg.be/sites/](https://www.vlaamsewaterweg.be/sites/default/files/2025-06/Economische%20schade%20van%20droogte%20voor%20de%20binnenvaart%20in%20Vlaanderen.pdf)
654 [default/files/2025-06/Economische%20schade%20van%20droogte%20voor%](https://www.vlaamsewaterweg.be/sites/default/files/2025-06/Economische%20schade%20van%20droogte%20voor%20de%20binnenvaart%20in%20Vlaanderen.pdf)
655 [20de%20binnenvaart%20in%20Vlaanderen.pdf](https://www.vlaamsewaterweg.be/sites/default/files/2025-06/Economische%20schade%20van%20droogte%20voor%20de%20binnenvaart%20in%20Vlaanderen.pdf)

656 Dembélé, M., Hrachowitz, M., Savenije, H. H. G., Mariéthoz, G., & Schaefli, B. (2020).
657 Improving the Predictive Skill of a Distributed Hydrological Model by Calibration
658 on Spatial Patterns With Multiple Satellite Data Sets. *Water Resources Research*,
659 56(1), e2019WR026085. <https://doi.org/10.1029/2019WR026085>

660 Demirel, M., Koch, J., Rakovec, O., Kumar, R., Mai, J., Müller, S., Thober, S., Samaniego,
661 L., & Stisen, S. (2024). Tradeoffs between temporal and spatial pattern calibration
662 and their impacts on robustness and transferability of hydrologic model parameters
663 to ungauged basins. *Water Resources Research*, 60(1). [https://doi.org/https :](https://doi.org/https://doi.org/10.1029/2022WR034193)
664 [//doi.org/10.1029/2022WR034193](https://doi.org/10.1029/2022WR034193)

665 Dirmeyer, P. A., Guo, Z., & Gao, X. (2004). Comparison, validation, and transferability of
666 eight multiyear global soil wetness products. *Journal of Hydrometeorology*, 5(6),
667 1011–1033. <https://doi.org/10.1175/JHM-388.1>

668 Dorigo, W., Xaver, A., Vreugdenhil, M., Gruber, A., Hegyiova, A., Sanchis-Dufau, A. D.,
669 Zamojski, D., Cordes, C., Wagner, W., & Drusch, M. (2013). Global automated
670 quality control of in situ soil moisture data from the international soil moisture
671 network. *Vadose Zone Journal*, 12(3), vzj2012–0097. [https://doi.org/10.2136/](https://doi.org/10.2136/vzj2012.0097)
672 [vzj2012.0097](https://doi.org/10.2136/vzj2012.0097)

673 Dorigo, W., Himmelbauer, I., Aberer, D., Schremmer, L., Petrakovic, I., Zappa, L., Preimes-
674 berger, W., Xaver, A., Annor, F., Ardö, J., et al. (2021). The international soil
675 moisture network: Serving earth system science for over a decade. *Hydrology and*
676 *Earth System Sciences Discussions*, 2021, 1–83. [https://doi.org/10.5194/hess-25-](https://doi.org/10.5194/hess-25-5749-2021)
677 [5749-2021](https://doi.org/10.5194/hess-25-5749-2021)

678 DOV. (2025). Databank Ondergrond Vlaanderen: Actuele grondwaterstandindicator [Ac-
679 cessed 27 Oct 2025].

- 680 Duniway, M. C., Petrie, M. D., Peters, D. P. C., Anderson, J. P., Crossland, K., &
681 Herrick, J. E. (2018). Soil water dynamics at 15 locations distributed across a
682 desert landscape: Insights from a 27-yr dataset. *Ecosphere*, 9(7), e02335. <https://doi.org/10.1002/ecs2.2335>
683
- 684 Erpicum, M., Nouri, M., & Demoulin, A. (2018). The Climate of Belgium and Luxem-
685 bourg. In A. Demoulin (Ed.), *Landscapes and Landforms of Belgium and Luxem-*
686 *bourg* (pp. 35–41). Springer International Publishing. [https://doi.org/10.1007/978-](https://doi.org/10.1007/978-3-319-58239-9_3)
687 [3-319-58239-9_3](https://doi.org/10.1007/978-3-319-58239-9_3)
- 688 Farr, T. G., Rosen, P. A., Caro, E., Crippen, R., Duren, R., Hensley, S., Kobrick, M., Paller,
689 M., Rodriguez, E., Roth, L., et al. (2007). The shuttle radar topography mission.
690 *Reviews of geophysics*, 45(2).
- 691 Feddes, R. (1982). Simulation of field water use and crop yield. In *Simulation of plant*
692 *growth and crop production* (pp. 194–209). Pudoc. <https://edepot.wur.nl/172222>
- 693 Filipović, V., Weninger, T., Filipović, L., Schwen, A., Bristow, K. L., Zechmeister-
694 Boltenstern, S., & Leitner, S. (2018). Inverse estimation of soil hydraulic properties
695 and water repellency following artificially induced drought stress. *Journal of Hy-*
696 *drology and Hydromechanics*, 66(2), 170–180. [https://doi.org/10.2478/johh-2018-](https://doi.org/10.2478/johh-2018-0002)
697 [0002](https://doi.org/10.2478/johh-2018-0002)
- 698 Ford, T. W., & Quiring, S. M. (2019). Comparison of Contemporary In Situ, Model,
699 and Satellite Remote Sensing Soil Moisture With a Focus on Drought Monitor-
700 ing. *Water Resources Research*, 55(2), 1565–1582. [https://doi.org/10.1029/](https://doi.org/10.1029/2018WR024039)
701 [2018WR024039](https://doi.org/10.1029/2018WR024039)
- 702 García-Herrera, R., Garrido-Perez, J. M., Barriopedro, D., Ordóñez, C., Vicente-Serrano,
703 S. M., Nieto, R., Gimeno, L., Sorí, R., & Yiou, P. (2019). The European 2016/17
704 Drought. *Journal of Climate*, 32(11), 3169–3187. [https://doi.org/10.1175/JCLI-D-](https://doi.org/10.1175/JCLI-D-18-0331.1)
705 [18-0331.1](https://doi.org/10.1175/JCLI-D-18-0331.1)
- 706 Gimbel, K. F., Puhlmann, H., & Weiler, M. (2016). Does drought alter hydrological
707 functions in forest soils? *Hydrology and Earth System Sciences*, 20(3), 1301–1317.
708 <https://doi.org/10.5194/hess-20-1301-2016>
- 709 Goudenhoofdt, E., & Delobbe, L. (2013). Statistical Characteristics of Convective Storms
710 in Belgium Derived from Volumetric Weather Radar Observations. *Journal of*
711 *Applied Meteorology and Climatology*, 52(4), 918–934. [https://doi.org/10.1175/](https://doi.org/10.1175/JAMC-D-12-079.1)
712 [JAMC-D-12-079.1](https://doi.org/10.1175/JAMC-D-12-079.1)
- 713 Hargreaves, G. H., & Samani, Z. A. (1985). Reference crop evapotranspiration from
714 temperature. *Applied engineering in agriculture*, 1(2), 96–99. [https://doi.org/10.](https://doi.org/10.13031/2013.26773)
715 [13031/2013.26773](https://doi.org/10.13031/2013.26773)
- 716 Hari, V., Rakovec, O., Markonis, Y., Hanel, M., & Kumar, R. (2020). Increased future
717 occurrences of the exceptional 2018–2019 Central European drought under global
718 warming. *Scientific Reports*, 10(1), 12207. [https://doi.org/10.1038/s41598-020-](https://doi.org/10.1038/s41598-020-68872-9)
719 [68872-9](https://doi.org/10.1038/s41598-020-68872-9)

- 720 Hartmann, J., & Moosdorf, N. (2012). The new global lithological map database glim: A
721 representation of rock properties at the earth surface. *Geochemistry, Geophysics,*
722 *Geosystems, 13*(12). <https://doi.org/10.1029/2012GC004370>
- 723 Ionita, M., Nagavciuc, V., Kumar, R., & Rakovec, O. (2020). On the curious case of the
724 recent decade, mid-spring precipitation deficit in central Europe. *npj Climate and*
725 *Atmospheric Science, 3*(1), 49. <https://doi.org/10.1038/s41612-020-00153-8>
- 726 Jarvis, N. (1989). A simple empirical model of root water uptake. *Journal of Hydrology,*
727 *107*(1-4), 57–72. [https://doi.org/10.1016/0022-1694\(89\)90050-4](https://doi.org/10.1016/0022-1694(89)90050-4)
- 728 Journée, M., Delvaux, C., & Bertrand, C. (2015). Precipitation climate maps of Belgium.
729 *Advances in Science and Research, 12*(1), 73–78. [https://doi.org/10.5194/asr-12-](https://doi.org/10.5194/asr-12-73-2015)
730 [73-2015](https://doi.org/10.5194/asr-12-73-2015)
- 731 Koster, R. D., Guo, Z., Yang, R., Dirmeyer, P. A., Mitchell, K., & Puma, M. J. (2009).
732 On the nature of soil moisture in land surface models. *Journal of Climate, 22*(16),
733 4322–4335. <https://doi.org/10.1175/2009JCLI2832.1>
- 734 Kumar, R., Musuza, J. L., Van Loon, A. F., Teuling, A. J., Barthel, R., Ten Broek, J., Mai,
735 J., Samaniego, L., & Attinger, S. (2016). Multiscale evaluation of the Standardized
736 Precipitation Index as a groundwater drought indicator. *Hydrology and Earth*
737 *System Sciences, 20*(3), 1117–1131. <https://doi.org/10.5194/hess-20-1117-2016>
- 738 Kumar, R., Samaniego, L., & Attinger, S. (2013). Implications of distributed hydrologic
739 model parameterization on water fluxes at multiple scales and locations. *Water*
740 *Resources Research, 49*(1), 360–379. <https://doi.org/10.1029/2012WR012195>
- 741 Kumar, R., Samaniego, L., Thober, S., Rakovec, O., Marx, A., Wanders, N., Pan, M., Hesse,
742 F., & Attinger, S. (2025). Multi-Model Assessment of Groundwater Recharge
743 Across Europe Under Warming Climate. *Earth's Future, 13*(1), e2024EF005020.
744 <https://doi.org/10.1029/2024EF005020>
- 745 Le sillon Belge. (2019). Une indemnisation pour les agriculteurs victimes de la sécheresse
746 2018. [https://www.sillonbelge.be/5310/article/2019-12-18/une-indemnisation-](https://www.sillonbelge.be/5310/article/2019-12-18/une-indemnisation-pour-les-agriculteurs-victimes-de-la-secheresse-2018)
747 [pour-les-agriculteurs-victimes-de-la-secheresse-2018](https://www.sillonbelge.be/5310/article/2019-12-18/une-indemnisation-pour-les-agriculteurs-victimes-de-la-secheresse-2018)
- 748 Livneh, B., Kumar, R., & Samaniego, L. (2015). Influence of soil textural properties on
749 hydrologic fluxes in the Mississippi river basin. *Hydrological Processes, 29*(21),
750 4638–4655. <https://doi.org/10.1002/hyp.10601>
- 751 Meersmans, J., Van Weverberg, K., De Baets, S., De Ridder, F., Palmer, S., Van Wesemael,
752 B., & Quine, T. (2016). Mapping mean total annual precipitation in Belgium, by
753 investigating the scale of topographic control at the regional scale. *Journal of*
754 *Hydrology, 540*, 96–105. <https://doi.org/10.1016/j.jhydrol.2016.06.013>
- 755 Mishra, A. K., & Singh, V. P. (2010). A review of drought concepts. *Journal of Hydrology,*
756 *391*(1-2), 202–216. <https://doi.org/10.1016/j.jhydrol.2010.07.012>
- 757 Moravec, V., Markonis, Y., Rakovec, O., Kumar, R., & Hanel, M. (2019). A 250-Year Euro-
758 pean Drought Inventory Derived From Ensemble Hydrologic Modeling. *Geophysical*
759 *Research Letters, 46*(11), 5909–5917. <https://doi.org/10.1029/2019GL082783>

- 760 Nachtergaele, F., van Velthuizen, H., Verelst, L., Wiberg, D., Henry, M., Chiozza, F.,
761 Yigini, Y., Aksoy, E., Batjes, N., Boateng, E., et al. (2023). *Harmonized world soil*
762 *database version 2.0*. FAO.
- 763 Nicholson, S. (2000). Land surface processes and Sahel climate. *Reviews of Geophysics*,
764 38(1), 117–139. <https://doi.org/10.1029/1999RG900014>
- 765 Nicolai-Shaw, N., Hirschi, M., Mittelbach, H., & Seneviratne, S. I. (2015). Spatial repre-
766 sentativeness of soil moisture using in situ, remote sensing, and land reanalysis
767 data. *Journal of Geophysical Research: Atmospheres*, 120(19), 9955–9964. <https://doi.org/10.1002/2015JD023305>
- 769 Peng, C., Zeng, J., Chen, K.-S., Ma, H., Letu, H., Zhang, X., Shi, P., & Bi, H. (2025).
770 Spatial Representativeness of Soil Moisture Stations and Its Influential Factors at a
771 Global Scale. *IEEE Transactions on Geoscience and Remote Sensing*, 63, 1–15.
772 <https://doi.org/10.1109/TGRS.2024.3523484>
- 773 Peng, L., Sheffield, J., Wei, Z., Ek, M., & Wood, E. F. (2024). An enhanced Standardized
774 Precipitation–Evapotranspiration Index (SPEI) drought-monitoring method inte-
775 grating land surface characteristics. *Earth System Dynamics*, 15(5), 1277–1300.
776 <https://doi.org/10.5194/esd-15-1277-2024>
- 777 Piézométrie du Service Public de Wallonie. (2025). La Piézométrie en Wallonie.
- 778 Rakovec, O., Mizukami, N., Kumar, R., Newman, A. J., Thober, S., Wood, A. W., Clark,
779 M. P., & Samaniego, L. (2019). Diagnostic Evaluation of Large-Domain Hydro-
780 logic Models Calibrated Across the Contiguous United States. *Journal of Geo-*
781 *physical Research: Atmospheres*, 124(24), 13991–14007. [https://doi.org/10.1029/](https://doi.org/10.1029/2019JD030767)
782 [2019JD030767](https://doi.org/10.1029/2019JD030767)
- 783 Rakovec, O., Samaniego, L., Hari, V., Markonis, Y., Moravec, V., Thober, S., Hanel, M.,
784 & Kumar, R. (2022). The 2018–2020 Multi-Year Drought Sets a New Benchmark
785 in Europe. *Earth's Future*, 10(3), e2021EF002394. [https://doi.org/10.1029/](https://doi.org/10.1029/2021EF002394)
786 [2021EF002394](https://doi.org/10.1029/2021EF002394)
- 787 Řehoř, J., Brázdil, R., Rakovec, O., Hanel, M., Fischer, M., Kumar, R., Balek, J., Poděbrad-
788 ská, M., Moravec, V., Samaniego, L., et al. (2025). Global catalog of soil moisture
789 droughts over the past four decades. *Hydrology and Earth System Sciences*, 29(14),
790 3341–3358. <https://doi.org/10.5194/hess-29-3341-2025>
- 791 Royal Forestry Society of Belgium. (2025). Belgium's forests in figures [Last accessed 02
792 Sep 2025].
- 793 Samaniego, L., Thober, S., Kumar, R., Wanders, N., Rakovec, O., Pan, M., Zink, M.,
794 Sheffield, J., Wood, E. F., & Marx, A. (2018). Anthropogenic warming exacerbates
795 European soil moisture droughts. *Nature Climate Change*, 8(5), 421–426. <https://doi.org/10.1038/s41558-018-0138-5>
- 797 Samaniego, L., Kumar, R., & Attinger, S. (2010). Multiscale parameter regionalization of
798 a grid-based hydrologic model at the mesoscale. *Water Resources Research*, 46(5),
799 2008WR007327. <https://doi.org/10.1029/2008WR007327>

- 800 Samaniego, L., Kumar, R., & Jackisch, C. (2011). Predictions in a data-sparse region
801 using a regionalized grid-based hydrologic model driven by remotely sensed data.
802 *Hydrology Research*, 42(5), 338–355. <https://doi.org/10.2166/nh.2011.156>
- 803 Samaniego, L., Kumar, R., & Zink, M. (2013). Implications of Parameter Uncertainty on
804 Soil Moisture Drought Analysis in Germany. *Journal of Hydrometeorology*, 14(1),
805 47–68. <https://doi.org/10.1175/JHM-D-12-075.1>
- 806 Seneviratne, S. I., Lüthi, D., Litschi, M., & Schär, C. (2006). Land–atmosphere coupling
807 and climate change in Europe. *Nature*, 443(7108), 205–209. <https://doi.org/10.1038/nature05095>
- 808
- 809 Sheffield, J., Goteti, G., Wen, F., & Wood, E. F. (2004). A simulated soil moisture based
810 drought analysis for the United States. *Journal of Geophysical Research: Atmo-*
811 *spheres*, 109(D24), 2004JD005182. <https://doi.org/10.1029/2004JD005182>
- 812 Shen, X., Liu, J., Han, X., Yang, H., Liu, H., & Ni, F. (2025). Modelling Infiltration Based
813 on Source-Responsive Method for Improving Simulation of Rapid Subsurface
814 Stormflow. *Water Resources Research*, 61(1), e2024WR037487. <https://doi.org/10.1029/2024WR037487>
- 815
- 816 Shrestha, P., Samaniego, L., Rakovec, O., Kumar, R., & Thober, S. (2025). A novel stream
817 network upscaling scheme for accurate local streamflow simulations in gridded
818 global hydrological models. *Water Resources Research*, 61(6), e2024WR038183.
819 <https://doi.org/10.1029/2024WR038183>
- 820 Sousa-Silva, R., Ponette, Q., Verheyen, K., Van Herzele, A., & Muys, B. (2016). Adapta-
821 tion of forest management to climate change as perceived by forest owners and
822 managers in Belgium. *Forest Ecosystems*, 3(1), 22. [https://doi.org/10.1186/s40663-](https://doi.org/10.1186/s40663-016-0082-7)
823 [016-0082-7](https://doi.org/10.1186/s40663-016-0082-7)
- 824 Statbel. (2025a). Land use [Last accessed 02 Sep 2025].
- 825 Statbel. (2025b). Population density.
- 826 Svoboda, M., LeComte, D., Hayes, M., Heim, R., Gleason, K., Angel, J., Rippey, B.,
827 Tinker, R., Palecki, M., Stooksbury, D., Miskus, D., & Stephens, S. (2002). THE
828 DROUGHT MONITOR. *Bulletin of the American Meteorological Society*, 83(8),
829 1181–1190. <https://doi.org/10.1175/1520-0477-83.8.1181>
- 830 Thibaut, K., Ayrat, P.-A., & Ozer, P. (2023). Development of the Chrono-Systemic Time-
831 line as a Tool for Cross-Sectional Analysis of Droughts—Application in Wallonia.
832 *Water*, 15(23), 4150. <https://doi.org/10.3390/w15234150>
- 833 Tröltzsch, J., Vidaurre, R., Bressers, H., Browne, A., La Jeunesse, I., Lordkipanidze,
834 M., Defloor, W., Maetens, W., & Cauwenberghs, K. (2016). Flanders: Regional
835 organization of water and drought and using data as driver for change. In H.
836 Bressers, N. Bressers, & C. Larrue (Eds.), *Governance for drought resilience: Land*
837 *and water drought management in europe* (pp. 139–158). Springer International
838 Publishing. https://doi.org/10.1007/978-3-319-29671-5_7

- 839 Van Loon, A. F., Kchouk, S., Matanó, A., Tootoonchi, F., Alvarez-Garreton, C., Hass-
840 aballah, K. E., Wu, M., Wens, M. L., Shyrokaya, A., Ridolfi, E., et al. (2024).
841 Drought as a continuum–memory effects in interlinked hydrological, ecological,
842 and social systems. *Natural Hazards and Earth System Sciences*, 24(9), 3173–3205.
843 <https://doi.org/10.5194/egusphere-2024-421>
- 844 Vicente-Serrano, S. M., Beguería, S., & López-Moreno, J. I. (2010). A Multiscalar Drought
845 Index Sensitive to Global Warming: The Standardized Precipitation Evapotran-
846 spiration Index. *Journal of Climate*, 23(7), 1696–1718. [https://doi.org/10.1175/](https://doi.org/10.1175/2009JCLI2909.1)
847 [2009JCLI2909.1](https://doi.org/10.1175/2009JCLI2909.1)
- 848 VMM. (2023). Toestand van het watersysteem [Accessed 6 Dec 2025].
- 849 Vonk, M. A. (2024). SPEI: A simple Python package to calculate and visualize drought
850 indices. <https://doi.org/10.5281/ZENODO.10816741>
- 851 Wang, A., Lettenmaier, D. P., & Sheffield, J. (2011). Soil Moisture Drought in China,
852 1950–2006. *Journal of Climate*, 24(13), 3257–3271. [https://doi.org/10.1175/](https://doi.org/10.1175/2011JCLI3733.1)
853 [2011JCLI3733.1](https://doi.org/10.1175/2011JCLI3733.1)
- 854 Wu, W., Geller, M. A., & Dickinson, R. E. (2002). The response of soil moisture to
855 long-term variability of precipitation. *Journal of Hydrometeorology*, 3(5), 604–613.
856 [https://doi.org/10.1175/1525-7541\(2002\)003<0604:TROSMT>2.0.CO;2](https://doi.org/10.1175/1525-7541(2002)003<0604:TROSMT>2.0.CO;2)
- 857 Xaver, A., Zappa, L., Rab, G., Pfeil, I., Vreugdenhil, M., Hemment, D., & Dorigo, W. A.
858 (2020). Evaluating the suitability of the consumer low-cost Parrot Flower Power
859 soil moisture sensor for scientific environmental applications. *Geoscientific Instru-*
860 *mentation, Methods and Data Systems*, 9(1), 117–139. [https://doi.org/10.5194/gi-](https://doi.org/10.5194/gi-9-117-2020)
861 [9-117-2020](https://doi.org/10.5194/gi-9-117-2020)
- 862 Xu, Z., Wu, Z., He, H., Guo, X., & Zhang, Y. (2021). Comparison of soil moisture at
863 different depths for drought monitoring based on improved soil moisture anomaly
864 percentage index. *Water Science and Engineering*, 14(3), 171–183. [https://doi.org/](https://doi.org/10.1016/j.wse.2021.08.008)
865 [10.1016/j.wse.2021.08.008](https://doi.org/10.1016/j.wse.2021.08.008)
- 866 Yang, Y., McVicar, T. R., Donohue, R. J., Zhang, Y., Roderick, M. L., Chiew, F. H., Zhang,
867 L., & Zhang, J. (2017). Lags in hydrologic recovery following an extreme drought:
868 Assessing the roles of climate and catchment characteristics. *Water Resources*
869 *Research*, 53(6), 4821–4837. <https://doi.org/doi:10.1002/2017WR020683>
- 870 Zhu, L., Gong, H., Dai, Z., Xu, T., & Su, X. (2015). An integrated assessment of the impact
871 of precipitation and groundwater on vegetation growth in arid and semiarid areas.
872 *Environmental Earth Sciences*, 74(6), 5009–5021. [https://doi.org/10.1007/s12665-](https://doi.org/10.1007/s12665-015-4513-5)
873 [015-4513-5](https://doi.org/10.1007/s12665-015-4513-5)
- 874 Zink, M., Kumar, R., Cuntz, M., & Samaniego, L. (2017). A high-resolution dataset
875 of water fluxes and states for germany accounting for parametric uncertainty.
876 *Hydrology and Earth System Sciences*, 21(3), 1769–1790.
- 877 Zreda, M., Desilets, D., Ferré, T. P. A., & Scott, R. L. (2008). Measuring soil moisture
878 content non-invasively at intermediate spatial scale using cosmic-ray neutrons.

